9

Hierarchical Cascades and the Single Fracture

Percolation and Seismic Detection

Laura J. Pyrak-Nolte, David D. Nolte, and Neville G. W. Cook

9.1. INTRODUCTION

The growing scarcity of water and petroleum, as well as the critical importance of establishing secure waste deposits that will not contaminate ground water, has focused attention on the technological and scientific difficulties of quantifying flow processes through porous or fractured media. Fractures and fracture networks are often the major conduits through which fluids and contaminants flow. Fracture networks are composed of associations of single fractures. In this sense, single fractures can be viewed as the primary building blocks. Before tackling the complex problem of flow through fracture networks, it is therefore essential to understand the physical properties of this basic unit, the single fracture, especially with regards to the effect of external perturbations such as stress on the flow properties of single fractures. Furthermore, it will be particularly useful if seismic methods can be used to predict the flow properties of intact fractures, without the need for expensive invasive coring and laboratory tests.

Fluid flow through a single fracture is complex because of the complex nature of the fracture void geometry. A natural fracture is composed of two rough surfaces in partial contact. Between the points of contact exist voids of variable aperture and geometry. When the fracture is subjected to stress, the fracture voids deform, resulting in an increase in contact area with a reduction in fracture void aperture and fracture void volume. These

Laura J. Pyrak-Nolte • Department of Civil Engineering and Geological Sciences, University of Notre Dame, Notre Dame, Indiana 46556-0767. *David D. Nolte* • Department of Physics, Purdue University, West Lafayette, Indiana 47907. *Neville G. W. Cook* • Department of Materials Science and Mineral Engineering and Earth Sciences Division, Lawrence Berkeley Laboratory, University of California, Berkeley, California 94720.

Fractals in Petroleum Geology and Earth Processes, edited by Christopher C. Barton and Paul R. La Pointe. Plenum Press, New York, 1995.

changes in void geometry influence both fracture deformation and fluid flow through the fracture.

Many investigators have attacked the problem of how the hydraulic and mechanical properties of fractures depend on aspects of fracture void geometry, often with an emphasis on the surface roughness of fractures. The roughness of fracture surfaces has been measured by Swan (1983), Barton *et al.* (1985), Brown and Scholz (1985 and 1986); Brown *et al.* (1986); and Brown (1987a,b). Methods that try to directly access the void space geometry, rather than inferring it, include measurement of the contact area of fractures using impression paper (Duncan and Hancock, 1966; Iwai, 1976; and Bandis *et al.*, 1983); measurement of the void space geometry using a metal injection technique (Pyrak-Nolte *et al.*, 1987; Pyrak-Nolte, 1991); epoxy injection techniques (Gale, 1987; Gentier *et al.*, 1989); or a water drop technique for measuring size and distribution of apertures (Hakami, 1988). These techniques all yield the same basic result: Void geometry in a fracture is variable in shape and size, and the geometry of the voids directly determines the deformation and fluid flow properties of a fracture. Exactly how the void space geometry influences fluid flow has been a point of much discussion.

Many investigators have modeled fracture void geometry and the relationship to flow properties using non-fractal models (Gangi, 1978; Patir and Cheng, 1978; Neuzil and Tracy, 1981; Tsang and Witherspoon, 1983; Sato *et al.*, 1984; Tsang, 1984; Schrauf and Evans, 1986; Muralidahr and Long, 1987; Rasmussen, 1987; Tsang and Tsang, 1987; Moreno *et al.*, 1988; Chen *et al.*, 1989; Shapiro and Nicholas, 1989; Silliman, 1989; Tsang and Tsang, 1989; Cook *et al.*, 1990) and fractal models (Brown, 1987; Pyrak-Nolte *et al.*, 1988; Wang and Narasimhan, 1988; Brown, 1989; Yang *et al.*, 1989). A fractal model of aperture correlations is described by Wang *et al.* (1988). A standard but overly simplified approach has been to model flow through a fracture as between parallel plates, that is, flow through the fracture is proportional to the cube of the fracture aperture; hence the cubic law (Iwai, 1976; Witherspoon *et al.*, 1980). It has been widely considered that such a basic approximation falls short in practice, and that more information concerning the geometry of the fracture is needed to better explain fracture flow properties. The key question is how to use the information of fracture void geometry to understand the fundamentals of fluid flow through fractures. Several investigators have used modified cubic laws to explain experimentally observed deviations from cubic law behavior. Iwai (1976) added an empirical factor to the cubic law to account for the effects of surface roughness. Engelder and Scholz (1981) found that their data agreed well with a cubic law modified to account for variable void cross-section as a result of applying stress. Several different investigators found that flow through a single fracture under high stress often yielded a relationship between flow and fracture aperture much greater than cubic (Iwai, 1976; Gale and Raven, 1980; Engelder and Scholz, 1981; Pyrak-Nolte *et al.*, 1987). Walsh (1981) concluded that flow rate depends on two factors: fracture aperture and tortuosity. Tortuosity is the effect of increasing the length of the flow path as contact area is increased. Examining the data of Kranz *et al.* (1979) he observed that the effect of tortuosity could be neglected for fluid flow because aperture is raised to the third power and therefore dominates the flow properties. In contrast, a computational study by Tsang (1984) concluded that tortuosity and surface roughness greatly affect the flow, especially when contact area is greater than thirty percent. Based on theoretical and experimental results, Cook *et al.* (1990) found that in-plane tortuosity effects are greater than out-of-plane tortuosity effects.

In this chapter, we address these sometimes contradictory aspects of fluid flow in

fractures by first modeling experimentally observed void space patterns with our stratified percolation construction, then using basic conclusions of percolation theory to give physical explanations. In Section 9.2, we describe the experimental data set consisting of hydraulic and mechanical properties of single fractures in several rock cores (Pyrak-Nolte *et al.*, 1987). Of particular importance is the measurement of the paths through which fluid flows through the fractures. A novel metal casting technique is employed that allows the void space geometries to be imaged and studied quantitatively. The void space patterns are fractal. In the following sections, we describe the stratified continuum percolation model (Nolte *et al.*, 1986; Pyrak-Nolte *et al.*, 1988; Nolte *et al.*, 1989; Nolte, 1989) that generates fractal void space geometries quantitatively similar to those observed in the experimental data of Pyrak-Nolte *et al.* (1987). We specifically use the concept of fractal dimensions (Mandelbrot, 1983) to quantify the seemingly random structure of the measured void space patterns. The fractal dimension measured in the laboratory is a parameter that must be fit by the percolation model. In this manner, the fractal dimension is more than merely a descriptive measure of the fracture geometry, but is used explicitly to determine percolation and flow properties through fractures.

Once the model is established, mechanical deformation of the fracture is approximated by assuming conservation of rock volume during fracture deformation. We find that the fluid flow through fractures is strongly dependent on the nonlinear relationships between fracture deformation and applied stress. Section 9.7 contains applications of the stratified continuum percolation model to examine the interrelationships among the hydraulic, seismic, and mechanical properties of a fracture, and to examine the apparent frequency dependence of fracture specific stiffness. We find that the hydraulic and seismic properties of a single fracture are linked through the specific stiffness of the fracture because fracture specific stiffness depends on the geometry of the fracture. A mechanism for a frequency-dependent stiffness is a simple consequence of the fracture void geometry because different frequencies sample different subsets of fracture specific stiffness.

9.2. HYDRAULIC AND MECHANICAL DATA

Pyrak-Nolte *et al.* (1987) performed hydraulic and mechanical tests on three core samples (E30, E32 and E35) of quartz monzonite measuring 52 mm in diameter by 77 mm in height. Each sample contained a single natural fracture orthogonal to the long axis of the core. These cores were obtained from extensometer holes from a waste isolation experiment in a drift in Stripa, Sweden, 340 m below the surface (Olkiewicz *et al.*, 1979). Hydraulic conductivity was measured for each of these samples as a function of axial loading, and changes in fracture void geometry and contact area were evaluated for samples E30 and E32.

Figure 9.1 contains the mechanical deformation data for all three samples as a function of stress. The measurements of fracture closure were made using linear variable differential transformers (LVDTs). The displacement, also called the closure, of the fracture under uniaxial stress is defined as the distance that LVDTs move for a given stress. It must be kept in mind that the LVDT displacement represents a far-field displacement, and not the local displacement of the fracture surfaces. The relationship between this far-field displacement and the actual change in the apertures of the fracture void spaces will be described later in this chapter in Section 9.5, "Conservation of Volume During Deformation." Though the

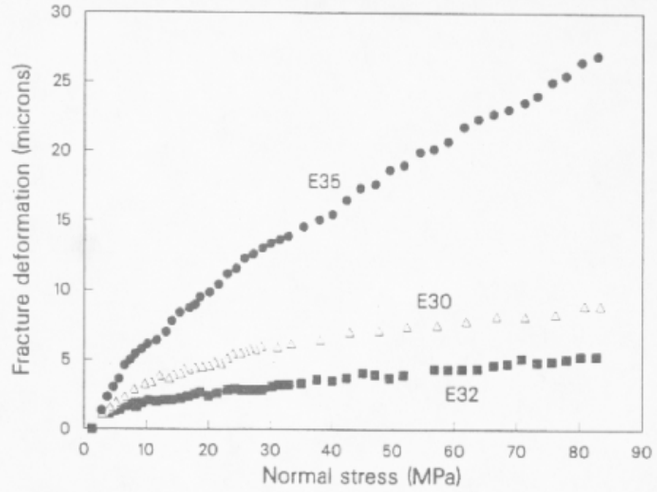

FIGURE 9.1. Fracture displacement as a function of normal stress for samples E35, E30, and E32 (Pyrak-Nolte *et al.*, 1987).

magnitude of fracture displacement varies for the different samples, all exhibit a rapid increase in displacement up to 10 MPa. Above 10 MPa, the increase in fracture displacement becomes more gradual. The displacement–stress curves in Fig. 9.1 need additional discussion because of their nonlinear behavior. It is obvious that for small stresses, stiffer fractures will displace less than will more compliant fractures. This is simply the definition of stiffness. However, for very high stresses the displacement asymptotically approaches a maximum value d_{max}. It is not at all obvious *a priori* that stiffer fractures should have a smaller maximum displacement than should more complaint fractures, but this is in fact what is observed in the data. This important point will also be emphasized and explained in Section 9.5.

The specific stiffness of each fracture was calculated from the displacement stress curves. The inverse of the tangent slopes to the displacement–stress curves defines the specific stiffness of the fracture. Values of specific stiffness for each fracture as a function of stress are shown in Fig. 9.2. Specific stiffnesses for all of the samples vary nonlinearly with stress, not with the linear relationship assumed by Walsh (1981). Specific stiffness increases rapidly with stress up to about 10 MPa and then increases more gradually. From the displacement–stress measurements, we see that there is a direct correspondence between maximum fracture displacement d_{max} and fracture stiffness. Fractures that displaced the least are stiffer than fractures that exhibited larger displacements. For example, E32 which displaced a maximum of 5.5 microns was the stiffest while fracture E35 which displaced a maximum of 28 microns is more compliant.

In experimental and theoretical studies of the flow properties of single fractures, the rate of fluid flow for a specific drop in head pressure is the measurable quantity. This is in contrast to permeabilities which are often defined and used when treating the flow of fluids through random media. However, in the case of single fractures, permeability cannot be defined uniquely because cross-sectional areas and flow lengths are ill-defined. Therefore,

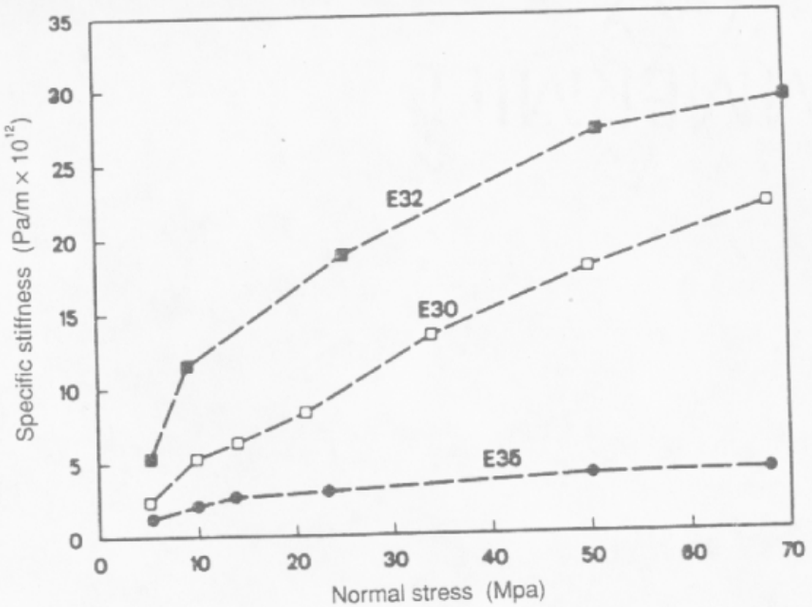

FIGURE 9.2. Specific stiffness for the three mechanical displacement tests shown in Fig. 9.1 (Pyrak-Nolte *et al.*, 1987).

in all of the discussions in this article we refer exclusively to flow rates per unit head, to avoid confusion from different possible definitions of permeability. Furthermore, we consider only laminar flow. Figure 9.3 contains the fluid flow data of Pyrak-Nolte *et al.* (1987) after values of irreducible flow were subtracted from the flow data. Irreducible flow is that flow that continues to flow even under the highest stresses. Pyrak-Nolte *et al.* (1987) found that flow through the three different fractures had a power-law relationship between flow and fracture displacement much greater than cubic: 8.3, 9.8, and 7.6, for E30, E32, and E35, respectively.

To better understand the flow process through fractures and the departure from the cubic law, Pyrak-Nolte *et al.* (1987) made measurements of the fracture void geometry for E30 and E32 as a function of stress. They used a metal casting technique in which molten Wood's metal (at 90°C) is injected into the fracture to make casts of the fracture voids. The fractured sample was placed under an axial load and evacuated to remove air from the void spaces. Molten metal then was injected from the perimeter of the sample. All void spaces that were connected to the sample perimeter were filled with the metal. It is possible that some void spaces may have been inaccessible from the perimeter, and these void spaces would appear as contact area. On the other hand, the injection pressure of the Wood's metal was 2 MPa which enables the metal to penetrate apertures as small as 100 nm. Therefore, we consider that the void spaces are faithfully being represented by the resulting metal casts. Once the void space patterns have been measured in this manner, it still remains to try to connect void space geometry with the flow path geometry. Voids filled by the metal may not participate in fluid flow. Figure 9.4 contains the composite photographs of the

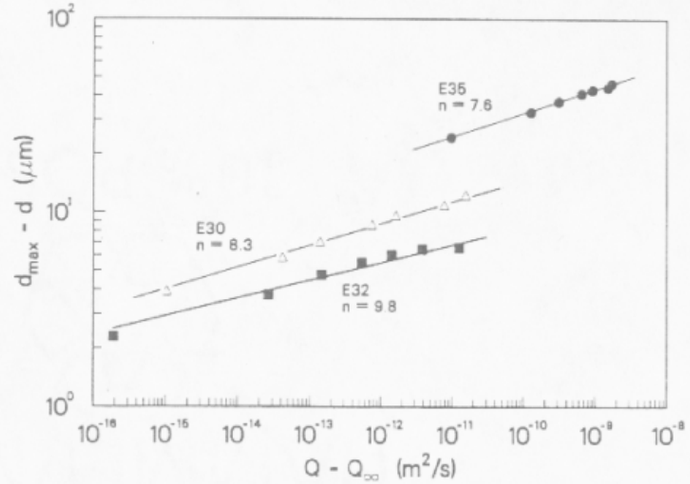

FIGURE 9.3. Fracture displacement versus flow per unit head drop after subtraction of irreducible flow for samples E35, E30, and E32 (Pyrak-Nolte *et al.*, 1987).

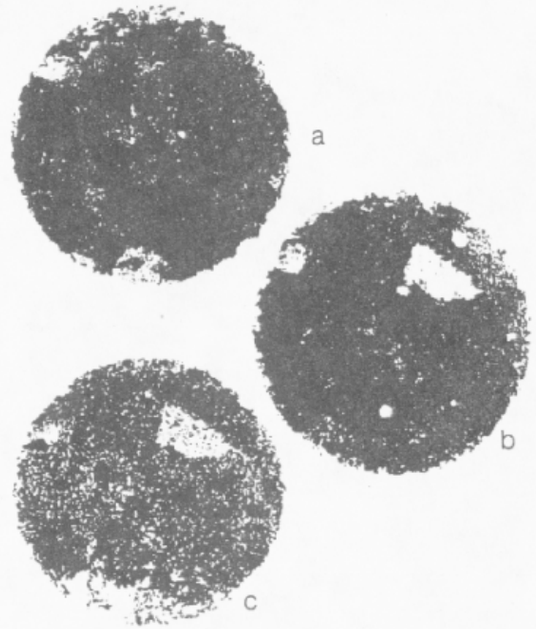

FIGURE 9.4. Composite photographs of entire fracture surface of sample E30 at three effective stresses: (a), 3 MPa; (b), 33 MPa; and (c), 85 MPa. White regions are contact area, black regions are flow paths (Pyrak-Nolte *et al.*, 1987).

entire fracture surface of sample E30 for three different stresses. Areas of white are contact area and areas of black are the void spaces along which the metal has penetrated. Figure 9.5 is a SEM (scanning electron microscope) composite micrograph of a small region of sample E30 when the sample was injected while under an effective stress of 85 MPa. At this high stress, there are still large areas of voids that remain open, thus allowing continued mechanical closure with increasing stress. However, the large voids are connected by small tortuous necks or channels which control the flow. Using a Zeiss image analyzer, measurements of the percent void space area as a function of stress were made based on the composite photographs. Figure 9.6 contains the graph of percent void space area as a function of stress for E30 and E32. E32 had much more contact area than E30.

From the combined data certain implicit relationships between mechanical and hydraulic properties are observed. First, flow through a fracture depends on the displacement of the fracture: fractures with larger maximum displacements have larger flow through the fracture. Second, a correspondence between contact area and fluid flow through the fracture is observed; as contact area increases, some flow paths are obstructed, thereby increasing the length of tortuous flow paths. Third, there exists a relationship between contact area and fracture stiffness; as more and more asperities come into contact with increasing stress, the stiffness of the fracture increases. Finally, an important relationship was observed in the data between fracture stiffness and fracture displacement [which is used by Bandis *et al.* (1983) for characterizing fractures]. Based on mechanical measurements,

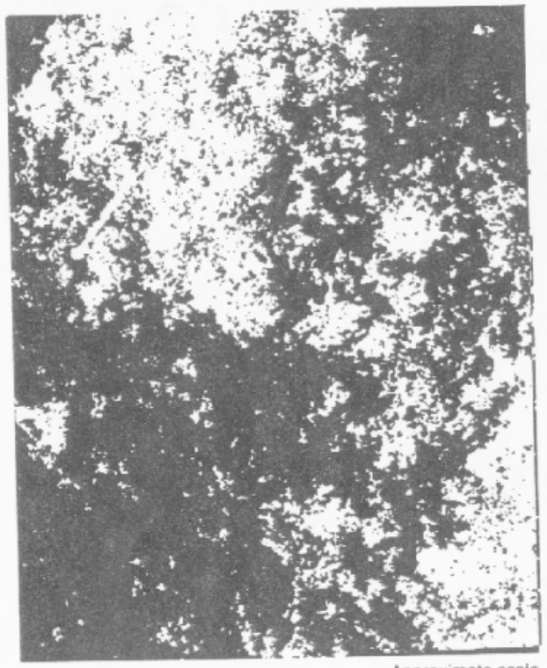

FIGURE 9.5. Composite micrograph from a portion of fracture surface of sample E30 for an effective stress of 85 MPa. White regions are contact area, black regions are flow paths (Pyrak-Nolte *et al.*, 1987).

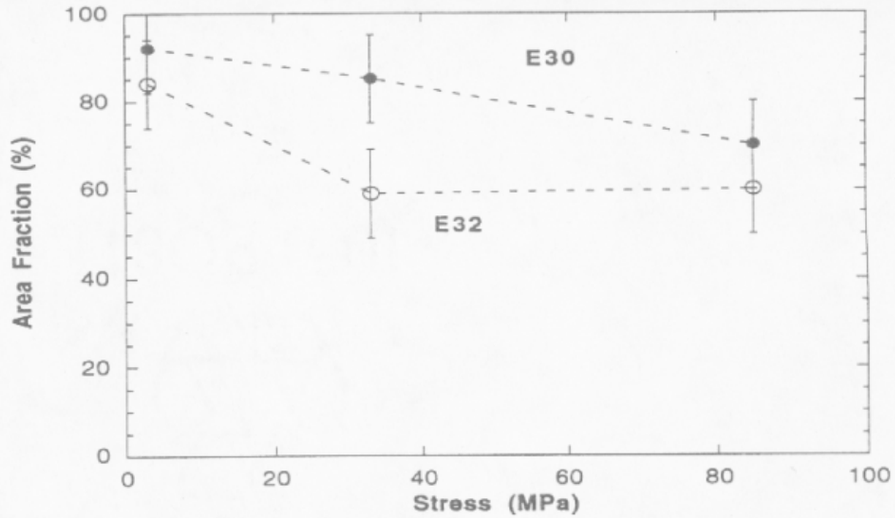

FIGURE 9.6. Percent flow path area as a function of stress for samples E30 and E32.

it was observed that fractures with the smallest maximum displacement d_{max} (hence smaller apertures) were the stiffest, while fractures which displaced the most were the most compliant. This relationship between fracture stiffness and fracture displacement is also observed in the data of Bandis *et al.*, 1983, and Gale 1987. These implicit relationships between mechanical and hydraulic properties arise because fluid flow and mechanical stiffness both depends on fracture aperture and contact area. This raises the possibility of predicting hydraulic properties of fractures based on measurements of fracture stiffness, obtained either from mechanical measurements performed on core samples, or by seismic transmission (Pyrak, 1988).

9.3. FRACTAL FLOW PATTERNS

One of the striking observations about the void space patterns is that they possess features on seemingly all length scales. The composite in Fig. 9.5 qualitatively retains many of the tortuous void space patterns independent of the scale of view. A fractal analysis reveals that the void space is self-similar. It is important to consider the usefulness of characterizing the seemingly random void spaces with a fractal dimension. The fractal dimension of a pattern gives a quantitative measure of the spatial correlations that exist in the pattern. Spatial correlations, in turn, arise from the physics of the pattern formation. In this case, the pattern formation originates with the fracture of the rock and the subsequent influx of fluid. As an example of spatial correlation, consider the void space geometry of the fracture. It is clear that a point of large aperture is surrounded by regions of large aperture, while points of contact are generally surrounded by other points of contact or low aperture. The void space patterns are therefore correlated. Mountains are another example. If a geologist stands at the peak of a mountain, there is a high probability that if he takes a

step, he will remain near the peak altitude. There is likewise a very low probability that after taking the step he will be at seal level. In the case of mountain ranges, erosion with gravity provides the physics behind the spatial correlation. Mile-high escarpments do not exist on Earth, because erosion and gravity pulls them down into talus slopes that lead more or less gradually from the mountain heights. On the other hand, mile-high escarpments can and do exist in weaker gravitational fields, such as on Miranda, one of the moons of Uranus, because the force of gravity there is considerably less. In short, spatial correlation reduces gradients and thereby reduces forces that form the pattern. It is therefore not surprising that the void geometry of fractures have spatial correlations. The question of why the spatial correlations should be scale-invariant still remains largely unsolved. However, it is now well established that many patterns formed through fragmentation in fact have self-similarity and therefore can be described by fractal dimensions. We will show shortly in this paper that the fractal dimension of the void spaces provides an important quantitative value which is used to generate percolation models to describe the effects of the fracture fractal geometry on fluid flow through the fracture. We first describe the measurement of the fractal dimension of the void space data.

The fractal dimensions of the void space composite photographs of specimens E30 and E32 were measured for stresses of 3, 33, and 85 MPa. For the experimental void space patterns, the contact areas were identified as tremas, and the distribution of trema sizes were related to the fractal dimension of the carpet. To measure the sizes of the tremas, or contact areas, a series of square grids were superposed on the void space pattern. The sizes of the grid cells started with the largest single cell that was contained within the pattern. If a contact area covered more than half of the cell, the cell was considered occluded. The cell size was then reduced in linear dimension by a factor of two, yielding four cells that covered the initial cell. Again, the number of cells that were occluded by a single contact area were tabulated. The process continues iteratively by reducing the linear dimension of the cells by a factor of two and tabulating the number of cells occluded. In this way the resolution of the grid is gradually increased, including progressively smaller areas of contact into the tabulations of the number of contact area versus their linear size. By plotting the logarithm of the number of cells which were not occluded (void space) against the logarithm of the linear size of the cells, the fractal dimension was obtained as the resulting slope of the plot. It should be noted that the above method is identical to the box-counting technique (see Feder, 1988), except for the definition of occlusion. In the box-counting technique, a box is occluded if it is entirely filled by a contact area, in contrast to our definition of at least fifty percent filling. This difference in definition only shifts the upper cutoff, but does not alter the fractal dimension. We chose our definition for convenience during the counting of boxes.

The fractal dimensions of the void space patterns as functions of stress are shown in Fig. 9.7 for specimen E30 and E32. The initial decrease of the fractal dimension at low stress is followed by an asymptotic approach to a fractal dimension near 1.95 at the highest stresses. It is significant that several of the physical properties of the fracture, when measured as functions of stress, yield asymptotic trends. An asymptotic relationship will be shown to exist between the far-field displacement of the fractured specimen and the closure of the void spaces in the fracture. This relationship is demonstrated through the development of the self-similar percolation model called stratified continuum percolation. This model also is successful in explaining the most salient features of fracture deformation and fluid flow through the fracture.

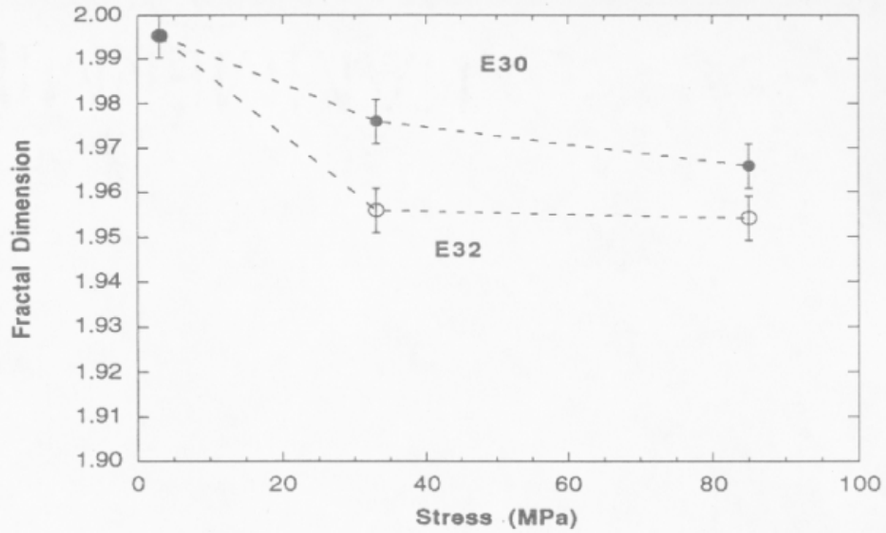

FIGURE 9.7. Fractal dimension of void spaces as a function of stress for samples E30 and E32.

9.4. STRATIFIED CONTINUUM PERCOLATION

Percolation studies have provided significant insight into the properties of flow through random media. A large body of literature exists on percolation theory and its applications [see Stauffer (1985) for a review]. Possibly the best understood percolation structures are two-dimensional random percolation models. Continuum percolation is one example. A standard random continuum percolation plot is shown in Fig. 9.8. This pattern consists of 5000 squares plotted at random locations within the large square area. The pattern is said to percolate if a continuous path can be found that spans the figure from top to bottom or side to side. Continuum percolation has a well-defined percolation threshold. This threshold is expressed as the amount of area that is occupied by the black squares when a percolating path first can be found across the pattern. This threshold is $A_c = 0.71$.

Given the success and understanding of percolation properties, it would be a great help to relate the experimental void space geometry to percolation models. However, a comparison between the standard random continuum percolation plot in Fig. 9.8 with the micrographs in Figs. 9.5 and 9.6 points out a clear discrepancy. The experimental patterns are not entirely random, but have a large degree of correlation. This correlation produces the clumped structures in Fig. 9.5, as compared to the filamentary and homogeneous patterns of Fig. 9.8. Stated another way, the experimental micrograph exhibits a fractal geometry, while the random percolation pattern does not. To model the experimental data, and to retain a percolation construction that will allow us to apply percolation theory results, we combined standard random continuum percolation with a recursive construction to yield fractal percolation patterns. We call the resulting hierarchical cascade stratified continuum percolation (Nolte *et al.*, 1989; Nolte, 1989).

Stratified percolation patterns are constructed recursively as a hybrid between standard random continuum percolation and a random Sierpinski carpet. The Sierpinski carpet provides the correlated skeleton upon which successively smaller tiers of standard percola-

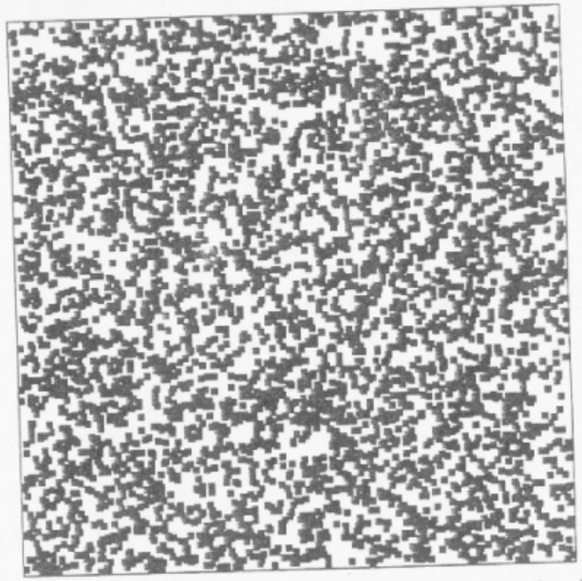

FIGURE 9.8. Standard random continuum percolation pattern, with 5000 squares plotted at random locations within the large square area. This pattern is close to the percolation threshold.

tion patterns are applied. The stratified percolation construction is demonstrated in Fig. 9.9. The construction begins by defining an initial large square region, called the first tier. This is the largest square in Fig. 9.9. Within this tier, N squares, with linear dimension reduced in scale by a factor b from the size of the first tier, are randomly laid down. These N smaller squares constitute the second tier, and are the second largest squares in Fig. 9.9. Just as in

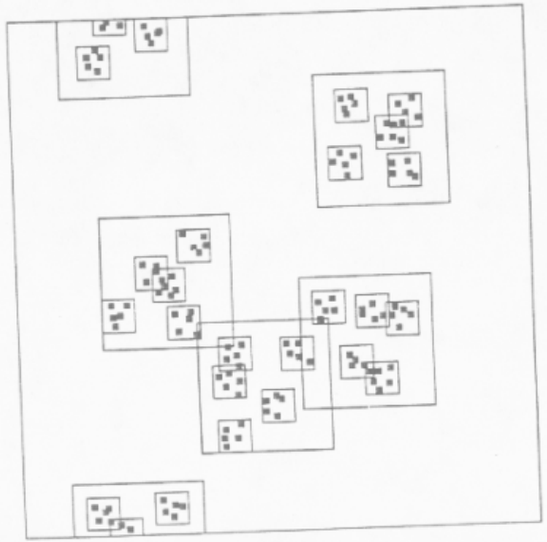

FIGURE 9.9. Cartoon of construction of pattern using stratified percolation model. This example has five points per tier for three tiers with a scale factor of 4.

standard random continuum percolation, these squares are allowed to overlap, as is seen in Fig. 9.9 for several of the squares. The construction continues recursively with N squares, reduced again by the scale factor b, placed within each of the squares making up the second tier. The recursive construction is terminated when the size of the square regions reaches a minimum cutoff. At this level, solid squares are plotted within the final tier. The stratified percolation pattern is defined by the final set of plotted squares. On the first tier, and only on the first tier, wraparound periodic boundary conditions are applied in which points positioned beyond a boundary of the first tier are plotted within the opposing boundary. The effect of this wraparound boundary condition is also seen in Fig. 9.9, where

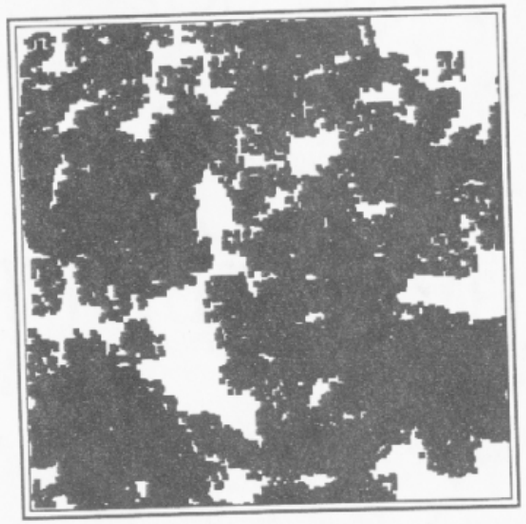

a

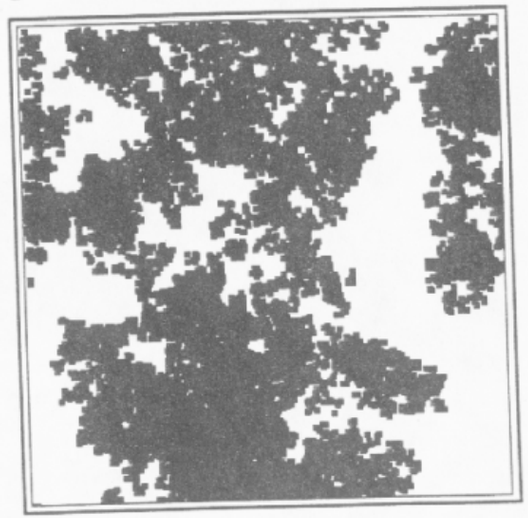

b

FIGURE 9.10. Stratified continuum percolation patterns for a different values of tiers and number of points per tier; (a), 3 tiers, $b = 4.2$, 30 points per tier, area fraction black = 0.81, fractal dimension $D = 1.984$; (b), 5 tiers, $b = 2.4$, 7 points per tier, area fraction black = 0.64, $D = 1.947$; (c), 5 tiers, $b = 2.4$, 9 points per tier, area fraction black = 0.89, $D = 1.990$; (d), 5 tiers, $b = 2.4$, 12 points per tier, area fraction black = 0.99, $D = 2.000$.

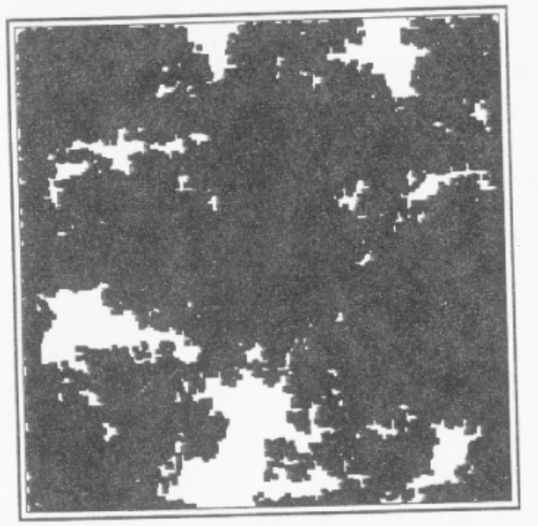

c

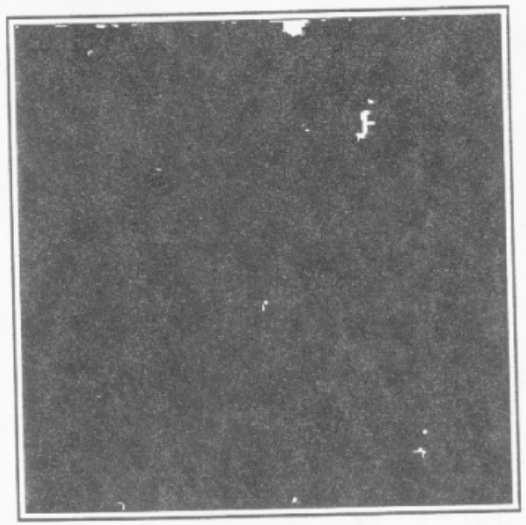

d

FIGURE 9.10. (*Continued*)

one of the second-tier squares and two of the third-tier squares have overhung the boundary of the first tier. Fig. 9.10 shows patterns generated from the stratified continuum percolation model for different numbers of tiers and different numbers of points per tier. The fractal dimensions of the resulting patterns were measured using the box-counting method (Feder, 1988).

As the model is presented this far, it is only a two-dimensional model in which a site is either occupied or not. Yet fracture void spaces are three-dimensional, with the height of the void space, the aperture, playing an essential role in fluid flow rates. To extend the stratified

percolation model into three dimensions, we have made the following conjecture: The aperture of the stratified percolation pattern is proportional to the density of sites. This conjecture cannot be justified *a priori*, but is reasonable for the following reason. The aperture distribution that results is explicitly correlated to the two-dimensional pattern: Apertures near the center of void spaces tend to be maximum, while apertures near the edges of the void space tend to be minimum. Furthermore, the distribution of apertures qualitatively resembles experimental aperture distributions. Figure 9.11 gives the aperture frequencies for the pattern in Fig. 9.10(d). The aperture frequency is approximately log-normal which has been observed experimentally for fractures in rock (Tsang, 1984; Gale, 1987; Hakami, 1988). It is important to note that the midpoint displacement model, which is also commonly used to obtain models of correlated terrain, does not yield a log-normal aperture distribution (Voss, 1988). Figure 9.12 shows the aperture contour plot for Fig. 9.10(d). The contours were made by averaging the aperture of a 6×6 pixel area. The white area represents contact area and increasing shades of gray to black represent increasing aperture. The scale of contour in Fig. 9.12 is 20 units of aperture per shade. We see that the patterns are highly clumped together and correlated.

The two-dimensional percolation properties of stratified continuum percolation have been described elsewhere (Nolte *et al.*, 1989; Nolte, 1989; Nolte and Pyrak-Nolte, 1991). Pyrak-Nolte *et al.* (1988) determined that the strong dependence of flow on fracture deformation could not be explained using only two-dimensional analysis. The role of the aperture distribution, and changes in the aperture distribution during deformation, must play an essential role in the dependence of fluid flow on fracture displacement. In understanding fluid flow through fractures, it is important to know how the flow paths will be affected as apertures are reduced by applied uniaxial stress. Figure 9.13(a) and (b)

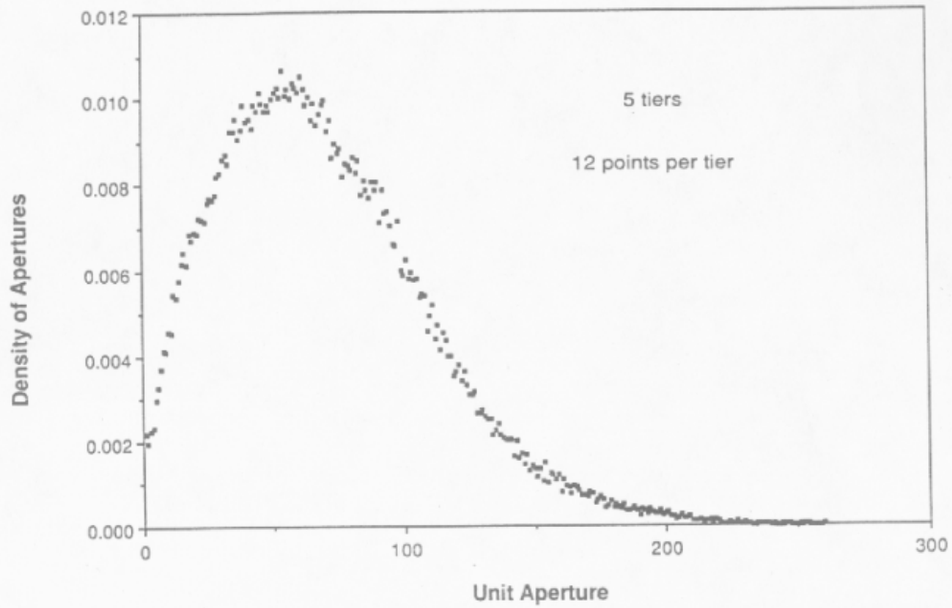

FIGURE 9.11. Graph of distribution of apertures for the pattern in Fig. 9.10(d).

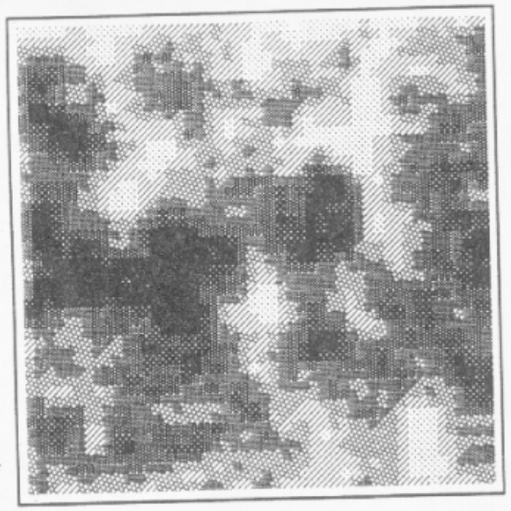

FIGURE 9.12. Aperture contour plot for pattern shown in Fig. 9.10(d). White represents contact area, and increasing shades of gray to black represents increasing aperture. Scale of contour: 20 units of aperture.

show the aperture contours when the apertures have been reduced. Stress here is considered only in terms of the reduction of aperture that is caused by an applied stress. The critical path and the critical neck of the pattern can be determined in this manner. The critical path is the path of highest aperture across the pattern. The critical neck is the smallest aperture along the critical path. For a reduction of 74 units of aperture, the critical path is quite evident and the critical neck can be seen in Fig. 9.13(b). The fractal dimension as a function of closure of aperture was calculated and is shown in Fig. 9.14 for the pattern in Fig. 9.10(d).

9.5. CONSERVATION OF VOLUME DURING DEFORMATION

Deformation of a natural fracture with applied stress is a complicated problem in geomechanics. Investigators have modeled the mechanical deformation of fractures by modeling the fracture as parallel plates separated by asperities of varying height (Greenwood and Williamson, 1966; Greenwood and Tripp, 1971; Gangi, 1978; Brown and Scholz, 1985, 1986; Hopkins *et al.*, 1987). To account for the deformation of the fracture, we assumed conservation of rock volume to account for the presence of asperities (Pyrak-Nolte *et al.*, 1988). In this assumption, the rock is considered as deformable yet incompressible. To understand our approach to the deformation of a fracture, consider the void geometry in Fig. 9.15. If the void space is reduced one unit of aperture, the asperities on either side also close by one unit of void aperture. The apparent missing volume of the asperity is distributed over the cross-section of the sample and added to the sample far from the fracture. Therefore as the apertures are closed by compressive stress, the average far-field displacement of the rock mass, d_{mech}, is less than the actual displacement of the void aperture, d_{void}. To develop the relation between far-field displacement and aperture closure, expressions for the void and contact areas are first derived from the aperture distribution as the void space is closed by the amount d_{void}. The distribution of apertures, $P(x)$, is defined through the relation

$P(x)\,dx$ = fraction of fracture area with apertures between x and $x + dx$.

a

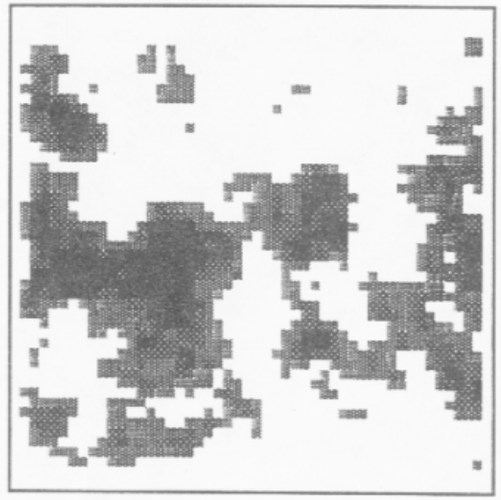

b

FIGURE 9.13. (a) Aperture contour for pattern shown in Fig. 9.10(d), for an aperture reduction of 40 units. Scale of contour: 20 units of aperture. (b) Aperture contour for pattern shown in Fig. 9.10(d), for an aperture reduction of 74 units. Scale of contour: 20 units of aperture.

The expressions for contact area and void area are

$$A_{\text{contact}}(d_{\text{void}}) = A\left\{\mathrm{P}(0) + \int_0^{d_{\text{void}}} P(x)\,dx\right\}$$

$$A_{\text{void}}(d_{\text{void}}) = A\int_{d_{\text{void}}}^{\infty} P(x)\,dx \qquad (1)$$

where A is the cross-sectional area of the fracture plane, and $P(0)$ is the zero-stress fraction of the contact area. Changes in the far-field displacement, $\delta(d_{\text{mech}})$, will be less than changes

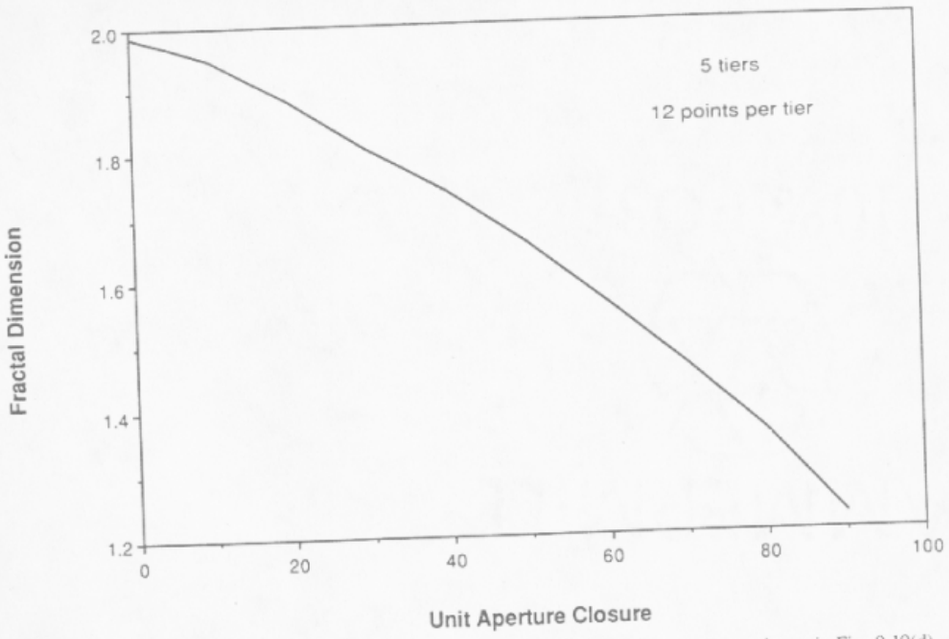

FIGURE 9.14. Fractal dimension as a function of unit closure of aperture for the pattern shown in Fig. 9.10(d).

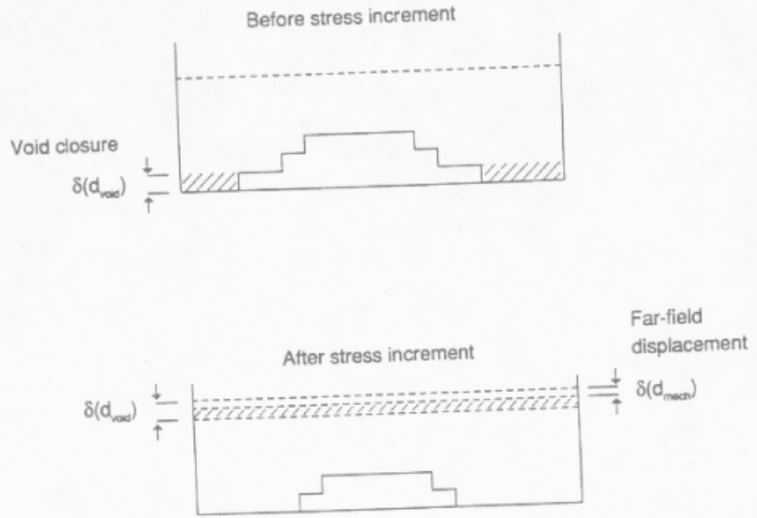

FIGURE 9.15. Application of principle of conservation of volume. For an incremental stress, the void space closes by $\delta(d_{void})$. The points of contact do not interpenetrate, but this mass is redistributed over the sample cross-section far from the fracture. The increment in the far-field mechanical displacement $\delta(d_{mech})$ is smaller than the void closure. This principle includes the basic feature of fracture deformation.

in the void aperture displacement, $\delta(d_{void})$, reduced by the ratio of the area of the void space to the cross-sectional area of the fracture plane:

$$A\,\delta(d_{mech}) = A_{void}(d_{void})\,\delta(d_{void}) \tag{2}$$

Equation (2) is the statement of conservation of volume. Integration yields the relationship between far-field displacement and void aperture closure

$$d_{mech}(d_{void}) = \frac{1}{A}\int_0^{d_{void}} A_{void}(y)\,dy \tag{3}$$

In the limit of high stress, the mechanical displacement, d_{mech}, approaches the asymptote defined by $d_{max} = d_{mech}(\infty) = V_{void}/A$, where d_{max} is the maximum mechanical displacement of the fracture (measured from the far field) and V_{void} is the zero-stress void volume of the fracture. The relationship between apparent fracture aperture and the closure of the void space apertures is shown in Fig. 9.16 for the pattern of Fig. 9.10(d). To generate this curve, for every unit closure of aperture, the mechanical displacement at the far field was calculated based on conservation of volume from Eq. (2). The straight line asymptote denotes the case where $d_{mech} = d_{void}$. There is clearly a nonlinear relationship between far-field mechanical displacement and void space aperture reduction, which will be reflected in the dependence of flow on mechanical displacement. The aperture of the critical neck is

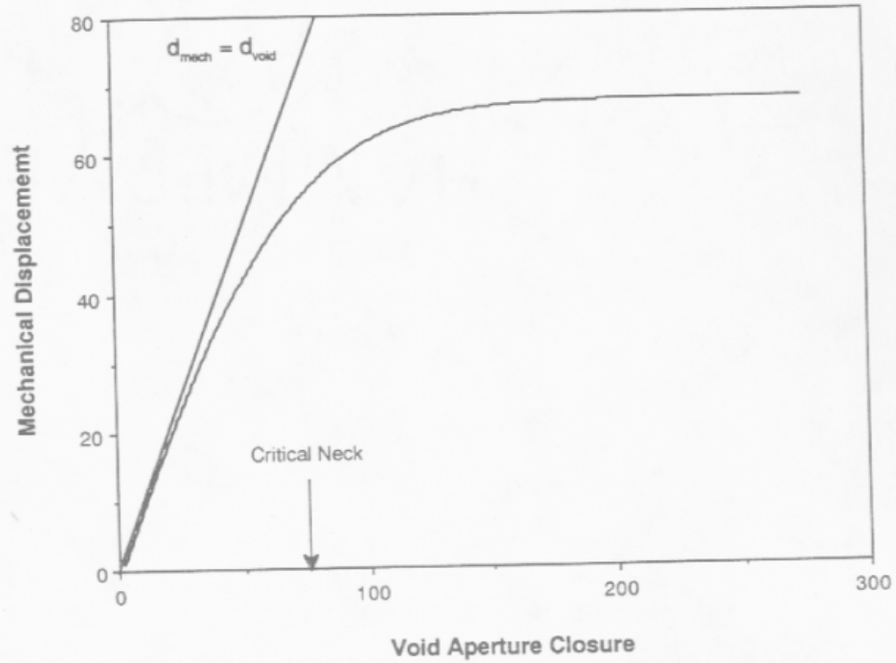

FIGURE 9.16. Mechanical displacement (apparent fracture aperture) versus aperture closure of the void space for pattern shown in Fig. 9.10(d). The nonlinear dependence is a result of the conservation of rock volume during deformation.

also shown in Fig. 9.16. This critical aperture is determined from the contours in Figs. 9.13(a) and (b) as the smallest aperture along the critical path.

9.6. FLUID FLOW DEPENDENCE ON MECHANICAL DISPLACEMENT

As stated above in the introduction, several investigations of fluid flow through natural fractures have found that flow depends on the apparent aperture of a fracture b raised to exponents considerably larger than cubic. This behavior is described by

$$Q - Q_\infty \propto (b)^n \propto (d_{max} - d_{mech})^n \tag{4}$$

where Q_∞ is the residual or irreducible flow. The effect of increasing contact area with increasing stress is implicitly included in Eq. (4) through the dependence of tortuosity on apparent aperture.

From the application of the principle of conservation of volume, a nonlinear relationship between mechanical (far-field) closure and void space closure was developed. The use of far-field displacement in Eq. (4), though convenient, would not be expected to yield a cubic law dependence of flow on mechanical fracture displacement.

Up to this point, we have made two simplifications. The first was the use of the stratified percolation construction to simulate the experimental void space. The second was the approximation of conservation of volume, applied to the stratified percolation patterns, to obtain the essential features of fracture deformation. Now we make a third simplifying assumption: flow through the fracture is determined entirely by the critical neck. This assumption is certainly an oversimplification, but we are attempting to obtain the essential behavior of the dependence of fluid flow on void space geometry. This assumption is partially justified by percolation studies of networks of nodes connected with inhomogeneous conductances. Several researchers (Ambegaoker *et al.*, 1971; Shklovskii and Efros, 1971; Pollak, 1972) found that the macroscopic conductivity is determined by the conductance of the elements that first create percolation across the distribution, i.e., the critical neck. Because flow depends locally on the cube of the aperture, and the apertures vary over an order of magnitude in the stratified percolation construction, the condition of strong heterogeneity is obeyed by the stratified percolation patterns. To find the qualitative behavior of the flow as a function of fracture deformation, we explicitly assume a cubic relationship between flow and the aperture of the critical neck. We will show, that despite the local dependence on the cubic law, the dependence of flow on mechanical displacement can yield exponents arbitrarily larger than cubic.

The relationship for flow through the critical neck is

$$Q - Q_\infty \propto (b_{crit})^3 \tag{5}$$

where b_{crit} is the aperture of the critical neck as a function of stress, and cubic dependence on the critical aperture has been explicitly assumed. As stress is increased, b_{crit} decreases until it is closed completely at the critical mechanical displacement d_{crit}. We continue to include irreducible flow Q_∞ because our assumption of conservation of volume is only an approximate way to include the deformation properties of the fracture. In practice, the void space will not close completely, even at high stresses (Hopkins and Cook, 1987) which may allow some residual fluid flow.

The dependence of flow on apparent aperture ($d_{max} - d_{mech}$) can now be plotted. This

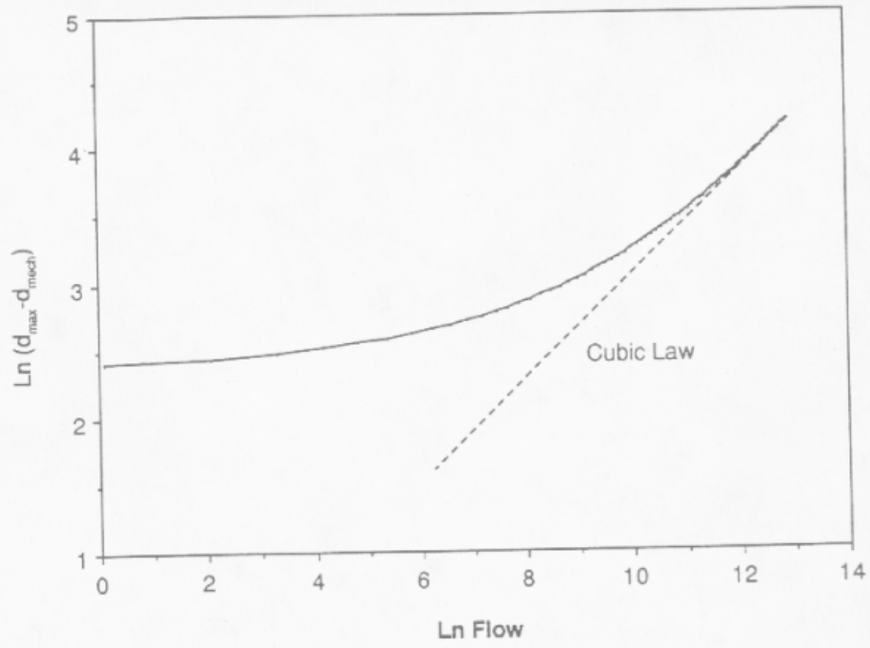

FIGURE 9.17. Log–log plot of apparent mechanical aperture ($= d_{max} - d_{mech}$, determined by the far-field displacement) versus flow for pattern shown in Fig. 9.10(d).

is displayed in the log–log plot in Fig. 9.17. The straight line shows the dependence expected from Eq. (4) for an exponent of three, labeled cubic law on the figure. At low stresses, i.e., high flow, the slope of the simulated curve approaches the slope of the cubic relationship. However, at even moderate stresses, the exponent (slope) increases significantly from cubic and can be arbitrarily large at high stresses.

The influence of each of our three assumptions on the results of Fig. 9.17 can now be discussed separately. Assumption 1 is that the stratified percolation construction provides a realistic representation of the fracture void space. The fractal dimension is adjusted to fit experimentally measured patterns. Assumption 2 is that conservation of rock volume during deformation is a simple yet important way to include the deformation mechanics of the asperities and surrounding rock mass. Deviations from cubic law dependence at low and moderate stresses result from the nonlinear relationship between far-field displacement and the closure of the void space, expressed in Eq. (2). Assumption 3 is that cubic-law flow dependence on the local microscopic aperture greatly simplifies the analysis and makes the connection with laminar fluid transport. The bound on the slope in Fig. 9.17 for low stresses is a direct consequence of this assumption. The dramatic deviation from cubic-law dependence at high stress (neglecting irreducible flow) is a consequence of the dominance of the critical neck on flow through the fracture. In conclusion, our three simplifications provide a simple and direct means of explaining the experimental dependence of flow through fractures on the mechanical deformation of the fracture, without reverting to heavy computation of either mechanical or hydraulic properties.

9.7. APPLICATIONS OF STRATIFIED CONTINUUM PERCOLATION

In this section, we demonstrate the application of the stratified continuum percolation model to examine (1), the interrelationship among fracture properties; and (2), the frequency dependence of fracture specific stiffness. The first application uses a unique data set collected for single natural fractures (Pyrak-Nolte *et al.*, 1987 and 1990) that has allowed interrelationships among the hydraulic, seismic, and mechanical properties of a fracture to be observed. The most important relationship is the correlation between fluid flow through a fracture and seismic attenuation caused by the fracture. This special relationship may enable seismic characterization of fractured sites to predict hydraulic response. Using the stratified percolation model to simulate fracture void geometry, the correlations between fluid flow and fracture specific stiffness were reproduced based on simple physical assumptions. It is shown that this correlation arises from the void geometry of the fracture, i.e. the contact area of the fracture and the aperture distribution of the fracture.

The second application of the stratified continuum percolation model examines the apparent frequency dependence of fracture specific stiffness. Fracture specific stiffness is the ratio of the increment of stress to the corresponding increment in fracture displacement produced by the closing of voids in the fracture. Static measurements of fracture specific stiffness yield lower values than those determined from dynamic techniques. Using the stratified continuum percolation model, a simple mechanism to explain the frequency dependent stiffness is investigated based on the void geometry of the fracture. Fracture specific stiffness can be frequency-dependent because different frequencies sample different subsets of the inhomogeneous distribution of stiffness that occurs in a fracture.

9.7.1. Interrelationships among Fracture Properties

Often a rock mass will contain fractures or sets of fractures that can be detected and located using seismic techniques. A key question is how the seismic signature of a fracture relates to its hydraulic properties. If there is a direct relationship between the seismic signature of a fracture and its hydraulic properties, then remote seismic techniques can be used to make hydrological assessments in the field without the need for expensive, multiple boreholes. Recently, several investigators have characterized and predicted the hydrologic properties of fractured rock masses from geological and geophysical data sets (Hesler *et al.*, 1990; Long *et al.*, 1991; Martel and Peterson, 1991; Martin *et al.*, 1990; Myer, 1991). However, direct evidence for shared hydraulic and seismic behavior has been lacking. To relate hydraulic and seismic properties, it is necessary to understand the role that fracture geometry plays in the hydraulic, seismic, and mechanical properties of single fractures. In the past, investigators have examined partial relationships between the mechanical and hydraulic properties of fractures, or between the mechanical and seismic properties of fractures. These studies have included the effects of fracture aperture and contact area on fluid flow through a fracture (Iwai, 1976; Engelder and Scholz, 1981; Walsh, 1981; Barton *et al.*, 1983; Tsang and Witherspoon, 1983; Brown, 1987b; Gale, 1987; Pyrak-Nolte *et al.*, 1987; Hakami, 1988; Chen *et al.*, 1989; Cook *et al.*, 1990), the effect of asperities or surface roughness on mechanical deformation (Greenwood and Williamson, 1966; Greenwood and Tripp, 1971; Gangi, 1978; Bandis *et al.*, 1983; Swan, 1983; Brown and Scholz, 1985 and 1986; Hopkins and Cook, 1987; Hopkins *et al.*, 1990; Yoshioka and Scholz, 1989), and the effect of fracture mechanical properties on wave propagation across a fracture (Morris

et al., 1964; Yu and Telvord, 1973; Kleinberg *et al.*, 1982; White, 1983; Medlin and Marsi, 1984; King *et al.*, 1986; Pyrak-Nolte *et al.*, 1990). Cook (1992) examined the hydraulic, mechanical, and seismic properties of joints by analyzing the deformation of asperities of contact and the voids between the asperities, i.e., the fracture geometry. Deformation of the asperities influences the joint closure, the fracture specific stiffness, and the aperture distribution in the fracture, and hence controls fluid flow and wave propagation across the fracture.

In this section, the relationships among fracture specific stiffness, fluid flow through the fracture, and apparent wave attenuation are investigated and compared with experimental data. The model used to examine the experimentally observed interrelationships among fracture properties (specifically the correlation between the hydraulic and seismic properties of natural fractures) consists of two parts. The stratified continuum percolation model is used to generate fracture void structures used to model the fluid flow through a fracture, the mechanical displacement of a fracture, and the fracture specific stiffness. A displacement discontinuity model is used to simulate the effect of a fracture on compressional and shear wave transmission (Pyrak-Nolte *et al.*, 1990). Fracture specific stiffness is identified as the primary link between the hydraulic and seismic characteristics of single fractures.

9.7.1.1. Experimentally Observed Interrelationships. The unique data set collected from single natural fractures (Pyrak-Nolte *et al.*, 1987 and 1990) in cores obtained at the Stripa site (Olkiewicz *et al.*, 1979) has made it possible to simultaneously correlate mechanical, hydraulic and seismic behavior among the fracture properties. The three quartz monzonite samples discussed in Section 9.2 were used in this investigation. The details of the experimental procedures can be found in references Pyrak-Nolte *et al.* (1987 and 1990). Mechanical displacement of the fractures (Fig. 9.1) and fluid flow through the fractures were measured for normal stresses ranging from 1.4 MPa to 85 MPa. For each sample, static fracture specific stiffness (Fig. 9.2) was determined from the stress–displacement data. The three fracture samples had differing static fracture stiffnesses (Fig. 9.1) and flow rates (Fig. 9.3). For the same range of normal stresses, compressional and shear wave transmission data across the fractures were measured and used to determine the dynamic stiffness of the fracture. In this analysis, the amplitudes of the transmitted signal from the fractured samples were normalized with respect to an intact specimen from an adjacent section of the drill core. The observation of the interrelationships among fracture properties was possible because the effect of the bulk rock, i.e. of the intact portions of the sample, was removed by the normalization. The interrelationships would be difficult to assess if the effect of bulk matrix porosity, bulk compressibility, and bulk seismic wave attenuation were present in the data sets.

The experimentally observed interrelationships among the hydraulic, mechanical, and seismic properties of a fracture are illustrated in Figs. 9.18–9.20. The observed relationships between fluid flow through the fractures and fracture specific stiffness (measured mechanically) for each sample is shown in Fig. 9.18. Significantly, the data from the three fractures fall near a single curve despite the differences in the mechanical and hydraulic properties among the fractures (Figs. 9.1–9.3). A clear systematic trend in the data is observed, i.e., compliant fractures support more fluid flow than fractures with a higher stiffness. A similar experimental relationship is observed between fluid flow through the fracture and the amplitudes of the transmitted compressional and shear waves, as shown in Figs. 9.19 and 9.20. Fractures with low attenuation exhibited a low flow rate. Again, the

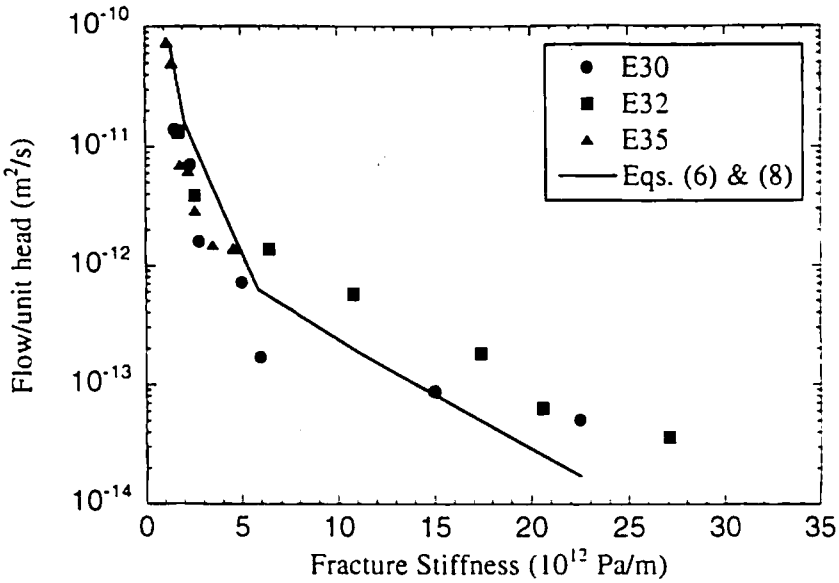

FIGURE 9.18. Comparison of the observed experimental relationship between fluid flow and fracture stiffness with the relationship determined from modeling using Eqs. 6 and 8.

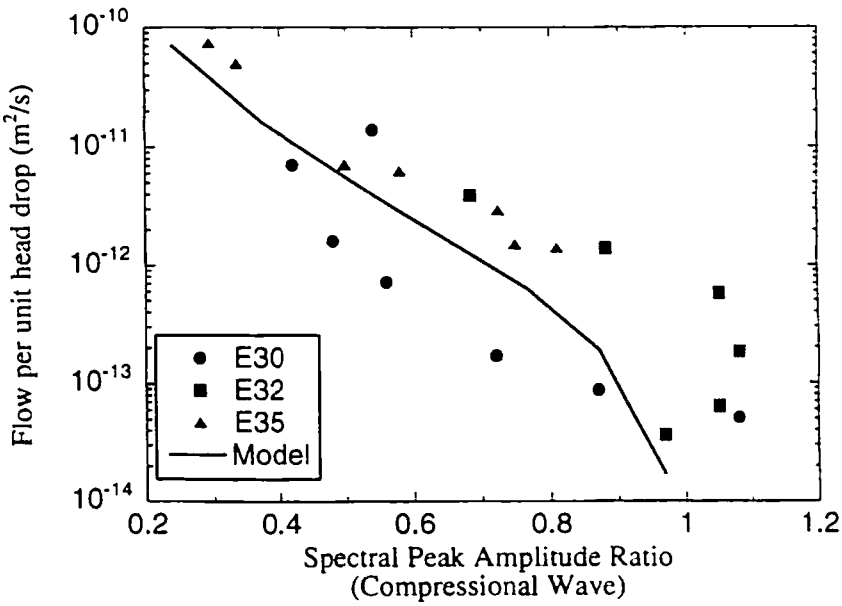

FIGURE 9.19. Relationship between compressional wave amplitude ratio and fluid flow through a fracture observed experimentally and determined from Eqs. 6, 8, and 13.

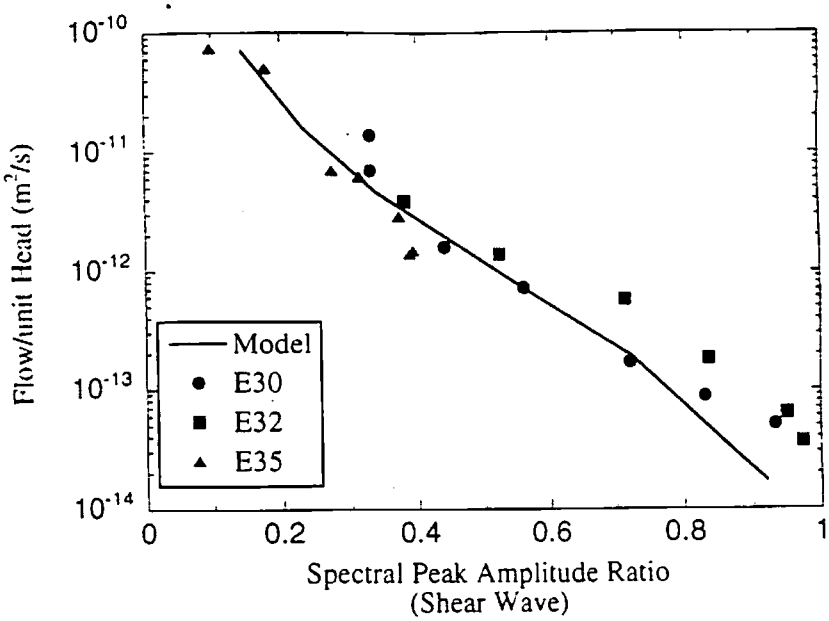

FIGURE 9.20. Relationship between shear wave amplitude ratio and fluid flow through a fracture observed experimentally and determined from Eqs. 6. 8, and 13.

data from the three fractures fall near a single curve. This suggests common statistical properties for the three samples which may reflect their common origin in the tectonic environment at Stripa.

9.7.1.2. Modeling Fluid Flow. To understand the empirical relationship between fluid flow through the fracture and wave propagation across the fracture, the stratified continuum model described above was used to generate fracture topologies. For this analysis, five-tier models were used with the number of points per tier (ppt) ranging from 7 ppt to 12 ppt. To simulate stress on a fracture, the number of points per tier is reduced which is equivalent to reducing the volume of the fracture. Low numbers of points per tier correspond to small fracture void volume. Conversely, high values correspond to large fracture void volume.

For a fracture with a variable aperture distribution, the critical neck dominates the macroscopic flow properties of the fracture, described in Eq. (5) of Section 9.6. The critical aperture, b_c, (critical neck) of a fracture is the smallest aperture on the path of largest apertures (critical path). Fluid flow through a critical neck is modeled as flow between parallel plates

$$Q = C_1 b_c^3 \tag{6}$$

where

$$C_1 = \frac{W}{12\mu}\frac{\Delta P}{\Delta L} \tag{7}$$

for rectangular flow. In Eq. (7), $\Delta P/\Delta L$ is the pressure gradient across the critical neck, μ is the viscosity, and W is the width of the critical neck through which fluid is flowing.

TABLE 9.1. Aperture of Critical Neck (b_c), Maximum Displacement (δ_{max}), and Standard Deviation of Asperity Height (σ) of Simulated Fracture Topologies for a Range of Number of Points per Tier (ppt)[a]

ppt	b_c	d_{max}	σ	ppt	b_c	d_{max}	σ
7	4	4.1	6.4	10	25	26.7	22.2
8	8	8.3	9.3	11	41	43.5	33.3
9	16	15.5	15.3	12	73	67.9	44.2

[a]This data is used to produce the model curves in Figs. 9.18–9.21.

Table 9.1 lists the critical apertures of the different stratified continuum patterns based on an average of five simulations for each number of points per tier. Equation (6) is used to calculate fluid flow through the simulated fracture using the values of b_c in Table 9.1. The constant C_1 in Eq. (6) was fit to the data and found to be $C_1 = 2.89 \times 10^{-16}$. These values of flow are used to construct the model curves in Figs. 9.18–9.20.

Static Fracture Specific Stiffness The specific stiffness of a fracture is defined as the ratio of an increment in stress to the increment of displacement caused by the deformation of the void space in the fracture. Fracture displacement and fracture specific stiffness depend on the surface roughness of the two fractures surfaces (Greenwood and Williamson, 1966; Brown and Scholz, 1985; Walsh and Grosenbaugh, 1979; Yoshioka and Scholz, 1989) and on the void geometry of the fracture (Hopkins and Cook, 1987; Hopkins *et al.*, 1990) when the two surfaces are in partial contact. In this analysis, fracture specific stiffness is taken to be inversely proportional to the maximum closure of the fracture, δ_{max}, at a given stress

$$K = \frac{C_2}{\delta_{max}} \tag{8}$$

where

$$\delta_{max}(\text{ppt}) = \frac{\text{Volume of voids (ppts)}}{\text{Cross-sectional area}} \tag{9}$$

and where C_2 is a constant of proportionality, and δ_{max} is a function of stress. Reducing the number of ppt of a pattern reduces the volume of the voids in the fracture and hence increases the stiffness of the fracture, Eq. (8). The maximum value of closure, δ_{max}, was determined using the principles of conservation of volume (Pyrak-Nolte *et al.*, 1988). Other investigators (Greenwood and Williamson, 1966; Greenwood and Grosenbaugh, 1979; Brown and Scholz, 1985; Yoshioka and Scholz, 1989) assume that fracture stiffness is inversely proportional to σ, the standard deviation in asperity height. The fracture stiffness determined from the asperity distribution is approximately linearly proportional to the fracture stiffness determined from the void volume, Eq. (8).

Relationship between Fluid Flow and Static Fracture Stiffness For fluid flow through the fracture to be related to the specific stiffness of the fracture, the critical aperture of the fracture, b_c, and the displacement δ_{max} must be related. Fracture stiffness is a function of far-field displacement, while flow depends on the actual apertures of the voids. Using the

stratified continuum model, the critical aperture was found to be approximately equal to δ_{max} of the fracture.

$$b_c \approx \delta(\text{ppt})_{max} \tag{11}$$

Eq. (11) is true for lognormal, Gaussian, and uniform distributions of apertures. Through this relationship, fracture specific stiffness and fluid flow through a fracture can be related. Substituting Eq. (11) into Eq. (8) and using Eq. (6) yields the equation relating fluid flow Q to the fracture stiffness K (Eq. 12).

$$K = \frac{C_2}{\sqrt[3]{Q/C_1}} \tag{12}$$

This relationship exists because fluid flow through the fracture and fracture stiffness both depend on fracture aperture. In addition, a power law relationship exists between fluid flow through the fracture and fracture stiffness. Fluid flow through the fracture is found to depend on the cubic power of fracture stiffness.

Table 9.1 lists the values of δ_{max}, σ, and b_c that were used to fit the experimentally observed relationship between fluid flow through a fracture and fracture specific stiffness (Fig. 9.18). The adjustable parameters are: number of points per tier (ppt); and C_1, C_2, and C_3 which are independent of ppt. The solid line in Fig. 9.18 is the fit to the data assuming $C_2 = 91.4 \times 10^{12}$. The fit to the experimental data (Fig. 9.18) suggests that Eq. (12) is valid. The results from the model characterize the basic trends observed in the data, i.e., fractures which support large values of fluid flow are more compliant. In addition, the curve is fit to the three different rocks, all from the same tectonic environment, and suggests a universal behavior for fractures in Stripa granite. Alternately, the common curve represented by all three fractures may signify that the three fractures obey subsets of a common fracture statistics that is applicable to all fractures in the Stripa waste isolation drift.

A comparison was made of the flow–stiffness relationship [using Eq. (8) for fracture stiffness] to the value of fracture stiffness determined from Equation (10). To use Eq. (10), it is necessary to calculate the stress, p, for each pattern. Increasing the stress on the fracture reduces the volume of the voids in the fracture. C_3 was fit to the data and assumed to be $C_3 = 30 \times 10^{12}$. In Fig. 9.18, the dashed-line curve represents the fit to the data using Eq. (10). This result fits the data at high stresses (large value of stiffnesses) but deviates at very low stresses.

Relationship between Fluid Flow and Seismic Behavior The displacement discontinuity model for wave propagation across a nonwelded interface has been used to simulate the seismic response of fractures and to predict dynamic fracture specific stiffness (Myer *et al.*, 1985; Pyrak-Nolte *et al.*, 1990). In this model, the fracture is represented by the following boundary conditions: (1), the stress across the fracture is continuous; and (2), displacements across the fracture are discontinuous. These boundary conditions were used by Mindlin (1960) and other investigators (Kendall and Tabor, 1971; Kitsunezaki, 1983; Murty, 1975; Pyrak-Nolte and Cook, 1987; Schoenberg, 1980) to study nonwelded contacts or fractures. The equation for the transmission coefficient for a wave propagated at normal incidence to a fracture is

$$|T| = \frac{1}{\sqrt{1 + \frac{\gamma^2}{K^2}}} \tag{13}$$

where

$$\gamma = \frac{\omega \rho c}{2} \tag{14}$$

ω is the angular frequency, ρ is the density of the rock, and c is the phase velocity of the rock. The values used to calculate γ for compressional and shear waves are listed in Table 9.2. The transmission coefficient is a function of the frequency and of the specific stiffness of the fracture. As the stiffness of the fracture increases, the amount of energy transmitted across the fracture increases.

Because fluid flow through the fracture is related to the stiffness of the fracture (Eq. 12), fluid flow through the fracture is related to the transmission coefficient of a wave propagated across a fracture. Equation (15) gives the form of this relationship by substituting Eq. (12) into Equation (13).

$$|T| = \frac{1}{\sqrt{1 + \dfrac{\gamma^2 (Q/C_1)^{2/3}}{C_2^2}}} \tag{15}$$

To fit the experimentally observed relationships of fluid flow as a function of P-wave amplitude and S-wave amplitude, the model values of b_c and δ_{max} (Table 9.1) are used with the values of ω, ρ, and c listed in Table 9.2. The model results were calculated using Eqs. 6, 8, and 15.

In Figures 9.19 and 9.20, the fluid-flow-amplitude dependence for all of the samples is compared to the results from the stratified percolation model and the displacement discontinuity model. Both the experimental data and the model results show a trend of decreasing fluid flow with an increase in the P-wave amplitude and S-wave amplitude. To obtain the best fit to the experimental results, it is necessary to increase the value of C_2. This is justified because dynamic stiffnesses are larger than static stiffnesses (Jaeger and Cook, 1979). The model curves in Figs. 9.19 and 9.20 assume $C_2 = 366 \times 10^{12}$ for compressional waves and $C_2 = 114 \times 10^{12}$ for shear waves. Based only on the geometry of the voids in the fracture, the models produce a good fit to the experimental data.

The correlation between fluid flow and fracture stiffness makes it possible to determine the hydraulic properties of a rock mass from seismic amplitudes and velocities. Fractures with a high apparent attenuation allow more fluid to flow than fractures that transmit more of the wave energy. For a constant stress, fractures with different hydraulic properties can be identified by their seismic signature.

The observed universal behavior of the experimental data leads to the interesting concept that data from a single core sample with a fracture contains all the information about

TABLE 9.2. Parameters for Modeling Wave Propagation across a Fracture

Density	2600 kg/m^3
Compressional wave velocity	5600 m/s
Shear wave velocity	3800 m/s
Frequency for shear wave	0.36 MHz
Frequency for compressional wave	0.46 MHz

the hydraulic, mechanical, and seismic properties of all of the fractures in the extended rock mass. For Stripa granite it is observed that a cubic relationship exists between fluid flow and fracture stiffness. Whether this dependence is true for fractures in other rock types and tectonic environment needs to be explored. While the results are for single fractures, all oriented perpendicular to the direction of stress and to the seismic wave front, and at the laboratory scale, these results should be extendible to fractures off-angle or fracture networks on the field scale.

9.7.2. *Frequency-Dependent Fracture Stiffness*

In modeling the interrelationships among fracture properties (Section 9.7.1.), the constant used to model static fracture stiffness had to be increased to match the dynamic response of the fracture. Jaeger and Cook (1979) have noted that static moduli of rock determined by static stress–strain measurements are lower in value than dynamic moduli. Frequency-dependent dynamical effects, such as frictional slip along internal interfaces (Walsh, 1966) have often been attributed to the observed difference in magnitude of the dynamic and static moduli. Pyrak-Nolte *et al.* (1990) observed that dynamic fracture specific stiffness of single natural fractures was greater in value than the statically determined values of fracture specific stiffness. Static specific stiffness of a fracture is determined from far-field displacement measurements as a function of static stress (Goodman, 1976; Bandis *et al.*, 1983). To determine dynamic specific stiffness of a fracture, the theoretical frequency-dependent transmission coefficient of the fracture is matched against experimentally measured transfer functions (Pyrak, 1988). From work performed on single natural fractures in the quartz-monzonite cores from the Stripa site, dynamic stiffnesses were determined to be typically three times larger than static stiffnesses (Pyrak-Nolte *et al.*, 1990). As in the case of bulk moduli, this difference between static and dynamic fracture stiffness has been attributed to dynamical effects. Such explanations are potentially important because they may be used to make conclusions concerning physical properties of fractures at the microscopic scale.

In this section, an alternate simple explanation for the larger values of dynamic stiffness compared to static stiffness is given, which demonstrates that the general frequency dependence of fracture stiffness can be related directly to an inhomogeneous distribution of stiffness across the fracture. This mechanism for frequency-dependent fracture stiffness is a simple consequence of the fracture void geometry. It is shown that fracture stiffness can be frequency dependent because different frequencies sample different subsets of fracture stiffness.

9.7.2.1. Theoretical Assumptions. The transmission coefficient for seismic wave propagation across a fracture from the displacement discontinuity model (see Pyrak-Nolte *et al.*, 1990, for a literature review) is given by Eqs. (13) and (14). The frequency dependence of the transmission coefficient arises from the inertia of the rock mass in response to the stress transmitted across the fracture through the fracture stiffness. If the fracture stiffness $\kappa \rightarrow \infty$, then $T \rightarrow 1$ and the fracture behaves as a welded interface. In the other extreme, as $\kappa \rightarrow 0$, then $T \rightarrow 0$ and all of the wave energy is reflected off the free surface. In general, the fracture acts as a low-pass filter, passing only those frequencies of the wave that are lower than the characteristic frequency $\omega_c = 2\kappa/Z$. Clearly, fractures with different stiffnesses will have different characteristic frequencies.

The formulation of the transmission coefficient given by Eq. (13) assumes a uniform

stiffness for the fracture. Real fractures, however, are strongly inhomogeneous and have complicated geometries. The asperities, points of contact, and apertures in a fracture consist of many different sizes and are distributed inhomogeneously over the interface. The spatial distribution and aperture of the voids control the stiffness of the fracture, and different regions of the fracture will have different stiffnesses. These local stiffnesses each define a different characteristic frequency ω_c. Some parts of the fracture will pass higher frequencies, while other parts will pass lower frequencies. This distribution of stiffnesses must be taken into account in the analysis of transmission of seismic waves across real fractures.

The following approximations are made to average over the transmission coefficients of different parts of a fracture: (1), the local transmission coefficient depends on the local static stiffness; and (2), regions of different stiffness transmit independently. The first approximately assumes that the local stiffness is defined as an average over length scales comparable to the wavelength. This assumption is valid if the asperity separation is smaller than the wavelength. Typical wavelengths for 10 MHz are 0.6 mm, compared to typical asperity separations of 0.5 mm (Brown *et al.*, 1986) for some fractures. Therefore the first approximation is valid for frequencies below 10 MHz. Also implicit in the first approximation is a local stiffness that is varying slowly with respect to a wavelength. Otherwise, the transmitted signal will experience attenuation by scattering. This additional assumption is plausible because real fracture asperity distributions are spatially correlated, meaning that there exist extended regions of similar asperity heights. The second approximation assumes that the total transmission of seismic wave amplitude is the incoherent sum of the transmitted amplitudes of individual regions. With this assumption, the forward transmission amplitude is calculated explicitly.

The transmission of seismic amplitudes is averaged over the fracture surface to calculate dynamic fracture stiffness. An integral-kernel equation is used to express the averaging process

$$T(\kappa(\omega),\omega) = \int_0^L \int_0^L T(\kappa(x,y),\omega)\, dx\, dy \tag{16}$$

where L is the length of a side of the fracture and the kernel $T(\kappa(x,y),\omega)$ is given by Eq. (16) with κ replaced by the spatially varying stiffness $\kappa(x,y)$. This expression implicitly defines a frequency-dependent fracture stiffness $\kappa(\omega)$ through

$$|T(\kappa(\omega),\omega)| = \left| \frac{1}{1 - i\dfrac{\omega Z}{2\kappa(\omega)}} \right| \tag{17}$$

and is easily inverted to yield

$$\kappa(\omega) = \frac{\omega Z |T|}{2\sqrt{1 - |T|^2}} \tag{18}$$

where $|T|$ is the magnitude of the averaged transmission coefficient given by Eq. (13).

9.7.2.2. Modeling of Frequency-Dependent Fracture Stiffness. The frequency dependence of fracture stiffness is investigated for stiffness distributions $\kappa(x,y)$ from the stratified continuum percolation model (Nolte *et al.*, 1989; Nolte and Pyrak-Nolte, 1991). For uniform and bimodal distributions of fracture stiffness see Pyrak-Nolte and Nolte

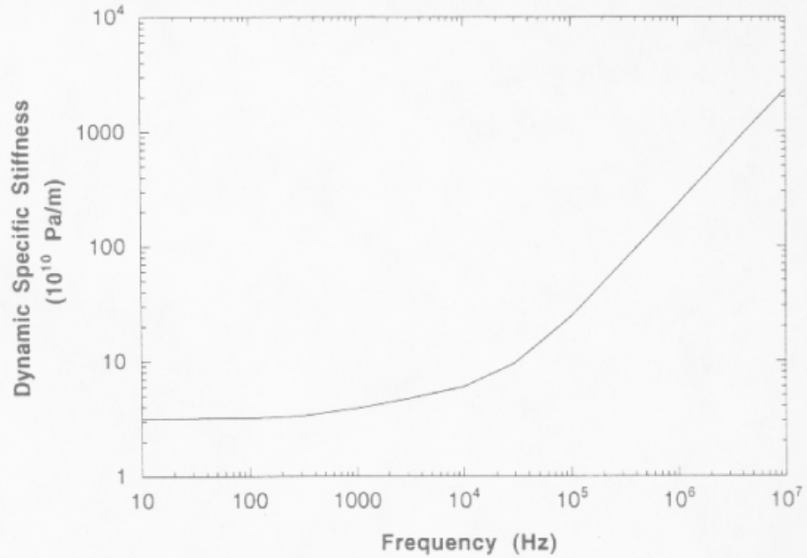

FIGURE 9.21. Frequency-dependent specific fracture stiffness as functions of frequency. The results for from a stratified fracture model are shown. The inhomogeneous stiffness distributions yield frequency dependent stiffnesses, with increasing stiffness for increasing frequency.

(1992). In the stratified fracture model, the local stiffness is assumed to vary inversely with the height of the asperities $b(x,y)$, i.e., $\kappa(x,y) = \alpha/b(x,y)$. This assumption is not crucial, but roughly reflects stress-displacement behavior for fractures. The dynamic fracture stiffness from Eq. (18) is shown in Fig. 9.21 as a function of frequency for the stiffness distribution given by the stratified continuum percolation model for an $\alpha = 1.0 \times 10^{12}$. A strong dependence of dynamic stiffness on frequency is observed for the stratified fracture model. The dynamic stiffness is equal to static fracture stiffness at low frequencies, but increases with increasing frequency. The increase in dynamic stiffness with frequency for the stratified aperture distribution reflects the change in the subset of stiffnesses sampled. Larger stiffnesses are sampled for higher frequencies.

9.7.2.3. Experimental Evidence of Frequency-Dependent Stiffness. To test this model for frequency-dependent fracture stiffness, compressional wave amplitude data are used from Pyrak-Nolte *et al.* (1990). Compressional waves with 1 MHz center frequency were propagated normal to the fracture plane. The experimental spectra in Fig. 9.22 show the transmitted amplitude as a function of frequency for a fracture. The experimental data were fit by simulating the fracture aperture distribution with the stratified percolation model. In the model, fracture apertures at different stresses are modeled by stratified continuum percolation patterns with 5 tiers with two adjustable parameters: the points per tier (ppt) and α. A ppt value of 8 was used for the data under 20 MPa stress, and a value of 9 was used for the data under 10 MPa. The apertures from the stratified percolation simulation are converted into specific stiffness values with $\alpha = 1.2 \times 10^{14}$ (for 10 MPA) and an $\alpha = 1.68 \times 10^{14}$ (for 20 MPa). The fits to the data are shown as the solid lines on Fig. 9.22. The fits are nearly perfect. In earlier work based on a uniform stiffness Pyrak-Nolte *et al.* (1990)

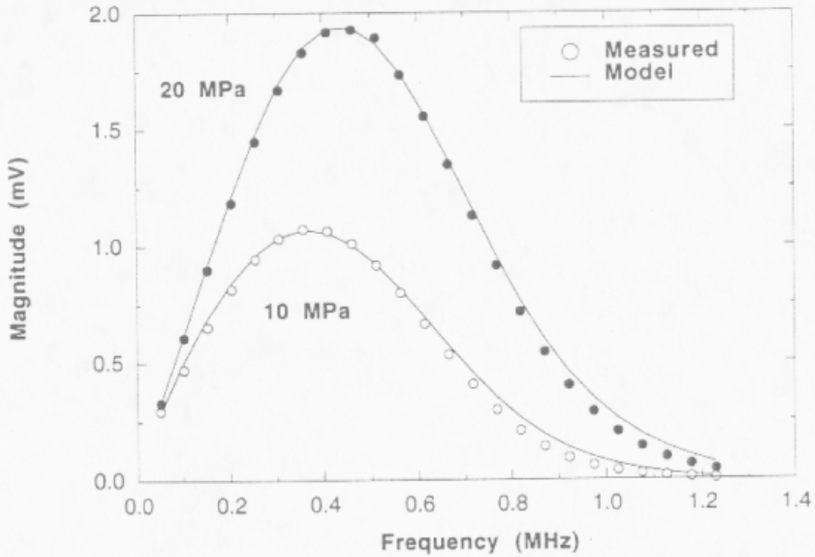

FIGURE 9.22. Transmitted compressional wave amplitudes as functions of frequency. The data points represent compressional wave spectral data from experiments on a fracture in granite (sample E30) subjected to stresses of 10 and 20 MPa. The solid curves represent fits using the stratified model and the frequency-dependent stiffness.

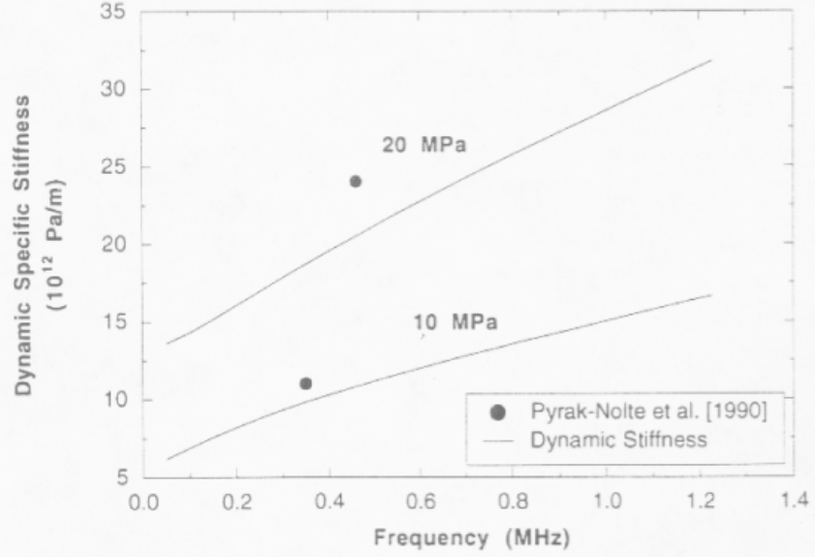

FIGURE 9.23. The dynamic stiffnesses (solid curves) as functions of frequency used to fit the data in Fig. 9.2. Solid dots represent the uniform stiffness and single frequency used by Pyrak-Nolte *et al.* (1990) to fit data.

fit a frequency-independent stiffness of 11×10^{12} Pa/m for a stress of 10 MPa and a stiffness of 24×10^{12} Pa/m for a stress of 20 Mpa. The frequency-dependent stiffness provides a significantly better fit to the data. The resulting dynamic stiffnesses from Eq. (18) are shown in Fig. 9.23 as functions of frequency. The values of uniform stiffness from Pyrak-Nolte *et al.* (1990) are the average of the stiffnesses predicted with the dynamic frequency model. The use of the stratified percolation model was motivated by previous success of the model. However, other possible aperture distributions cannot be ruled out based on the fit. The point was simply to demonstrate a plausible origin of the frequency-dependent fracture stiffness.

From this application of the stratified continuum percolation model, we have found that the frequency-dependent nature of fracture specific stiffness may be a simple consequence of the subset of apertures sampled by a given frequency. No additional dynamical effects need be invoked. However, it must be expressed that this is only one possible mechanism for a frequency-dependent fracture stiffness. It does not rule out additional dynamical effects such as locking or friction. Another interesting aspect of this discussion is the implicit relationship to scaling and fractals. For fractal or multifractal fracture topologies, there are no intrinsic length scales. This allows the wavelength of the elastic wave to define the length scale for the dynamic response of the system.

9.8. CONCLUSIONS

The scale-invariance of flow paths and contact areas in laboratory samples of rock fractures led us heuristically to propose a stratified continuum percolation model based on a hierarchical construction to simulate the topology of the void spaces between fracture surfaces. This construction has replicated many of the features of real fractures, such as correlated void spaces, characteristic log-normal aperture distributions, nonlinear stress-displacement behavior, and the strong dependence of flow rates on far field displacements. The attraction of the stratified percolation model is two-fold. First, it captures the essential properties of the void space and contact area that result from the genesis and subsequent evolution of fractures in rock. Second, it offers the prospect, through scale invariance, of translating the results of a study on a laboratory scale to the field scale.

Changes in fracture aperture as a result of changes in effective stress have been shown experimentally to have a profound and complex effect on fluid flow. Clearly, this derives from changes in void space topology brought about by deformation of the rock in the vicinity of the voids. In principle, for given mechanical properties of the rock, it is possible to calculate the changes in void geometry as a result of effective stress. In practice, such a calculation would be both computationally intensive and require an unreasonably detailed knowledge of the void geometry. Again, the question arises of whether or not a more simple model might capture the essential features of the phenomena involved. The essential process involved in the deformation is that the complex stress redistribution adjacent to the voids as a result of this deformation does not involve changes in the net volume of the rock in this region. Therefore, we chose to model changes in void aperture so that the volume of rock would be conserved. The volumetric change in void space is distributed across the whole projected area of the fracture to relate it to changes in measured fracture aperture. The final essential abstraction in our discussion of the dependence of flow on fracture void geometry derives from studies of percolation in networks of highly inhomogeneous conductances. The simple result of percolation theory is that resistance to

flow is dominated by the critical neck, the smallest aperture along the critical path of highest aperture through the void space.

Perhaps the most important conclusion in this article is our identification of a direct relationship between seismic attenuation by a fracture and its hydraulic properties. This result has immediate potential for characterizing the hydraulic properties of geotechnical sites using noninvasive seismic techniques. We were able to explain the trends using our fracture void geometry simulated by a hierarchical cascade. We were also able to explain a frequency-dependent fracture specific stiffness that is caused by sampling subsets of fracture stiffness.

Though the simple approach described here has been effective in simulating the behavior of some natural fractures in laboratory experiments, it remains to be established whether or not it is sufficiently effective and robust to describe a wider range of laboratory experiments and to form the basis for extending this work to the field. Clearly, the latter requires measurements, on a field scale, of the geometry of the void spaces and contact areas between fracture surfaces, of fluid flow through such fractures, and of the effects of stress or pore pressure on flow. Hopefully, it will be possible to characterize fractures in the field in such a way as to enable the properties of these fractures to be analyzed with a simple model described above.

ACKNOWLEDGMENTS

L. J. Pyrak-Nolte would like to acknowledge the Young Investigator award from the Division of Earth Sciences at the National Science Foundation. D. D. Nolte would like to thank the Alfred P. Sloan Foundation and the Presidential Young Investigator award from the Division of Materials Research at the National Science Foundation.

REFERENCES

Ambegaoker, V., Halperin, B. I., and Langer, J. S., Hopping conductivity in disordered systems, *Phys. Rev.* **B4**, 2612–2620 (1971).

Bandis, S. C., Lumsden, A. C., and Barton, N. R., Fundamentals of rock joint deformation, *Internat. J. Rock Mech. Mining Sci. Geomech. Abstr.* **20**, 6, 249–268 (1983).

Barton, N., Bandis, S., and Bakhtar, K., Strength, deformation and conductivity coupling of rock joints, *Internat. J. Rock Mech. Mining Sci. Geomech. Abstr.* **22**, 3, 121–140 (1985).

Brown, S. R., Fluid flow through rock joints: the effect of surface roughness, *J. Geophys. Res.* **92**, 1337–1347 (1987a).

Brown, S. R., A note on the description of surface roughness using fractal dimension, *Geophys. Res. Lett.* **14**, 11, 1095–1098 (1987b).

Brown, S. R., Transport of fluid and electric current through a single fracture, *J. Geophys. Res.* **94**, B7, 9429–9438 (1989).

Brown, S. R., and Scholz, C. H., Closure of random elastic surfaces in contact, *J. Geophys. Res.* **90**, 5531–5545.

Brown, S. R., and Scholz, C. H., Closure or rock joints, *J. Geophys. Res.* **91**, 4939–4948 (1986).

Brown, S. R., Kranz, R. L., and Bonner, B. P., Correlation between the surfaces of natural rock joints, *Geophys. Res. Lett.* **13**, 1430–1434 (1986).

Chen, D. W., Zimmerman, R. W., and Cook, N. G. W., The effect of contact area on the permeability of fractures, in: *Proceedings of the 30th U. S. Symposium on Rock Mechanics*, Morgantown, W. Va., June 19–22, 1989, 81–88.

Cook, N. G. W., Natural joints in rock: Mechanical, hydraulic and seismic behavior and properties under normal stress, *Internat. J. Rock Mech. Mining Sci. Geomech. Abstr.* **29**, 3, 198–223 (1992).

Cook, A.-M., Myer, L. R., Cook, N. G. W., and Doyle, F. M., The effects of tortuosity on flow through a natural fracture, in: *Proceedings of the 31st U. S. Rock Mechanics Symposium*, Boulder, Colorado, June, 1990, A.A. Balkema Publishers, Rotterdam, 371–378 (1990).

Duncan, N., and Hancock, K. E., The concept of contact stress in assessment of the behavior of rock masses as structural foundations, in: *Proceedings of First Congress of the International Society for Rock Mechanics*, Lisbon, **2**, 487–492 (1966).

Engelder, T., and Scholz, C. H., Fluid flow along very smooth joints at effective pressures up to 200 megapascals, in: *Mechanical Behavior of Crustal Rocks, The Handin Volume*, American Geophysical Union Monograph 24, pp. 147–152 (1981).

Feder, J., *Fractals*, Plenum Press, New York (1988).

Gale, J. E., Comparison of coupled fracture deformation and fluid flow models with direct measurements of fracture pore structure and stress–flow properties, in: *Proceedings, Rock Mechanics: Proceedings of the 28th U.S. Symposium*, Tucson, Arizona, pp. 1213–1222, June 1987, University of Arizona (1987).

Gale, J. E., and Raven, K. G., Effects of sample size on the stress–permeability relationship for natural fractures, Lawrence Berkeley Laboratory Report, LBL-11865 (SAC-48), Berkeley, California (1980).

Gangi, A. F., Variation of whole and fractured porous rock permeability with confining pressure, *Internat. J. Rock Mech. Mining Sci. Geomech. Abstr.* **15**, 249–257 (1978).

Gentier, S., Billaux, D., and van Vliet, L., Laboratory testing of the voids of a fracture, *Rock Mech. Rock Eng.* **22**, 149–157 (1989).

Goodman, R. E., *Methods of Geological Engineering*, West Publishing, St. Paul, Minn., 170–173 (1976).

Greenwood, J. A., and Williamson, J. B. P., Contact of nominally flat surfaces, *Proc. R. Soc., London Ser. A* **295**, 300–319 (1966).

Greenwood, J. A., and Tripp, J. H., The contact of two nominally flat rough surfaces, *Proc. Inst. Mech. Eng.* **185**, 625–633 (1971).

Hakami, E., Water flow in single rock joints, Ph.D. thesis, Lulea University of Technology, Sweden, p. 99 (1988).

Hesler, G. J., III, Zheng, Z., and Myer L. R., In-situ fracture stiffness determination, *Rock Mechanics Contributions and Challenges: 31st U. S. Rock Mechanics Symposium*, 405–411 (1990).

Hopkins, D. L., and Cook, N. G. W., Fracture stiffness and aperture as a function of applied stress and contact geometry, in: *Proceedings, Rock Mechanics: Proceedings of the 28th U. S. Symposium*, Tucson, Arizona, June 1987, University of Arizona, pp. 673–680 (1987).

Hopkins, D. L., Cook, N. G. W., and Myer, L. R., Normal joint stiffness as a function of spatial geometry and surface roughness, *Internal Symposium on Rock Joints*, A. A. Balkema Publishers, pp. 203–210 (1990).

Iwai, K., Fundamentals of fluid flow through a single fracture, Ph.D. thesis, Berkeley, University of California (1976).

Jaeger, J. C., and Cook, N. G. W., *Fundamentals of Rock Mechanics*, Chapman and Hall, London (1979).

Kendall, K., and Tabor, D., An ultrasonic study of the area of contact between stationary and sliding surfaces, *Proc. R. Soc., London, Ser. A*, **323**, 321–340 (1971).

King, M. S., Myer, L. R., and Rezowalli, J. J., Experimental studies of elastic-wave propagation in a columnar-jointed rock mass, *Geophys. Prospecting* **34**, 1185–1199 (1986).

Kitsunezaki, C., Behavior of plane waves across a plane crack, *J. Mining College Akita Univ., Ser. A* **6**, 173–187 (1983).

Kleinberg, R. L., Chow, E. Y., Plona, T. J., Orton, M., and Canady, W. J., Sensitivity and reliability of fracture detection techniques for borehole application, *J. Petroleum Tech.* **34**, 657–663 (1982).

Kranz, R. L., Frankel, A. D., Engelder, T., and Scholz, C. H., The permeability of whole and jointed Barre granite, *Internat. J. Rock Mech. Mining Sci. Geomech. Abstr.* **16**, 225–234 (1979).

Long, J. C. S., Karasaki, K., Davey, A., Peterson, J., Lansfeld, M., Kemeny, J., and Martel, S., An inverse approach to the construction of fracture hydrology models conditioned by geophysical data, *Internat. J. Rock Mech. Mining Sci. Geomech. Abstr.* **28**, 121–142 (1991).

Mandelbrot, B. B., *The Fractal Geometry of Nature*, W.H. Freeman and Company, New York (1983).

Martel, S. J., and Peterson, J. E., Jr., Interdisciplinary characterization of fracture systems at the US/BK site, Grimsel Laboratory, Switzerland, *Internat. J. Rock Mech. Mining Sci. Geomech. Abstr.* **28**, 295–323 (1991).

Martin, C. D., Davison, C. C., and Kozak, E. T., Characterizing normal stiffness and hydraulic conductivity of a major shear zone in granite, *Rock Joints*, Stephansson ed, A.A. Balkema, Rotterdam, 549–556 (1990).

Medlin, W. L., and Marsi, L., Laboratory experiments in fracture propagation, *Soc. Petroleum Eng. J.* **24**, 256–268 (1984).

Mindlin, R. D., Waves and vibrations in isotropic planes, in: *Structural Mechanics* (J. W. Goodier and W. J. Hoff, eds.), Pergamon Press, 199 (1960).

Moreno, L., Tsang, Y. W., Tsang, C. F., Hale, F. V., and Neretnieks, I., Flow and tracer transport in a single fracture: A stochastic model and its relation to some field observations, *Water Resources Res.* **24**, 2033–2048 (1988).

Morris, R. L., Grine, D. R., and Arkfeld, T. E., Using compressional and shear acoustic amplitude for the location of fractures, *J. Petroleum Tech.* **16**, 623–632 (1964).

Muralidahr, K., and Long, J. C. S., in: *Flow and Transport Through Unsaturated Fractured Rock* (D. D. Evans, and T. J. Nicholson, eds.), Geophysical Monograph 42, Washington, D.C., American Geophysical Union, pp. 115–120 (1987).

Murty, G. S., A theoretical model for the attenuation and dispersion of Stoneley waves at the loosely bonded interface of elastic half spaces, *Phys. Earth Planet. Int.* **11**, 65–79 (1975).

Myer, L. R., Hydromechanical and seismic properties of fractures, *7th International Congress on Rock Mechanics* **1**, 397–404 (1991).

Myer, L. R., Hopkins, D., and Cook, N. G. W., Effects of contact area of an interface on acoustic wave transmission characteristics, *26th U. S. Rock Mechanics Symposium* **1**, 565–572 (1985).

Neuzil, C. E., and Tracy, J. V., Flow through fractures, *Water Resources Res.* **17**, 191–199 (1981).

Nolte, D. D., Invariant fixed point in stratified continuum percolation, *Phys. Rev. A* **40**, 4817–4819 (1989).

Nolte, D. D., Pyrak-Nolte, L. J., and Cook, N. G. W., Fractal flow paths in rock and the approach to percolation (abstract), *EOS (Amer. Geophys. Union Trans.)* **67**, 871 (1986).

Nolte, D. D., Pyrak-Nolte, L. J., and Cook, N. G. W., The fractal geometry of flow paths in natural fractures in rock and the approach to percolation, *Pure Appl. Geophys.* **131**, 271 (1989).

Nolte, D. D., and Pyrak-Nolte, L. J., Stratified continuum percolation: scaling geometry of hierarchical cascades, *Phys. Rev. A* **44**, 6320–6333 (1991).

Olkiewicz, A., Gale, J. E., Thorpe, R., and Paulsson, B., Geology and fracture system at Stripa, Lawrence Berkeley Laboratory Report, LBL-8907 (SAC-21), Berkeley, California (1979).

Patir, N., and Cheng, S., An average flow model for determining effects of three-dimensional roughness on partial hydrodynamic lubrication, *J. Lubrication Technol.* **100**, 12–17 (1978).

Pollack, M., A percolation treatment of D.C. hopping conduction, *J. Non-Crystalline Solids* **11**, 1–24 (1972).

Pyrak, L. J., Seismic visibility of fractures, Ph.D. thesis, Berkeley, University of California (1988).

Pyrak-Nolte, L. J., and Cook, N. G. W., Elastic interface waves along a fracture, *Geophys. Res. Lett.* **14**, 1107–1110 (1987).

Pyrak-Nolte, L. J., Myer, L. R., Cook, N. G. W., and Witherspoon, P. A., Hydraulic and mechanical properties of natural fractures in low permeability rock, in: *Proceedings, International Society for Rock Mechanics, 6th International Congress on Rock Mechanics*, Montreal, Canada, August 1987, **1**, 225–231, A. A. Balkema, Rotterdam.

Pyrak-Nolte, L. J., Cook, N. G. W., and Nolte, D. D., Fluid percolation through single fractures, *Geophys. Res. Lett.* **15**, 1247–1250 (1988).

Pyrak-Nolte, L. J., Myer, L. R., and Cook, N. G. W., Transmission of seismic waves across single natural fractures, *J. Geophys. Res.* **95**, 8617–8638 (1990).

Pyrak-Nolte, L. J., Feasibility of using Wood's metal porosimetry techniques to measure the fracture void geometry of cleats in coal, Topical Report Gas Research Institute, GRI-91/0373 (1991).

Pyrak-Nolte, L. R., and Nolte, D. D., Frequency dependence of fracture stiffness, *Geophys. Res. Lett.* **19**, 325–328 (1992).

Rasmussen, T. C., Computer simulation model of steady fluid flow and solute transport through three-dimensional networks of variably saturated, discrete fractures, in: *Flow and Transport Through Unsaturated Fractured Rock* (D. D. Evans, and T. J. Nicholson, eds.), Geophysical Monograph 42, pp. 107–114, Washington D.C., American Geophysical Union (1987).

Sato, K., Watanabe, K., and Kotajima, N., Fundamental study on flow resistance in rock fissures, *Soils and Foundations* (Japan), **24**, 1–8 (1986).

Schoenberg, M., Elastic wave behavior across linear slip interfaces, *J. Acoust. Soc. Am.* **68**, 1516–1521 (1980).

Schrauf, T. W., and Evans, D. D., Laboratory studies of gas flow through a single natural fracture, *Water Resources Res.* **22**, 1038–1050 (1986).

Shapiro, A. M., and Nicholas, J. R., Assessing the validity of the channel model of fracture aperture under field conditions, *Water Resources Res.* **25**, 817–828 (1989).

Shklovskii, B. I., and Efros, A. L., Impurity band and conductivity of compensated semiconductors, *Soviet Physics-JETP* **33**, 468–474 (1971).

Silliman, S. E., An interpretation of the difference between aperture estimates derived from hydraulic and tracer tests in a single fracture, *Water Resources Res.* **25**, 2275–2283 (1989).

Stauffer, D., *Introduction to Percolation Theory*, Taylor and Francis, London (1985).

Stesky, R. M., Electrical conductivity of brine-saturated fractured rock, *Geophysics* **51**, 1585–1593 (1986).

Swan, G., Determination of stiffness and other joint properties from roughness measurements, *Rock Mech. Rock Eng.* **16**, 19–38 (1983).

Tsang, Y. W., and Witherspoon, P. A., The dependence of fracture mechanical and fluid flow properties on fracture roughness and sample size, *J. Geophys. Res.* **88**, 2359–2366 (1983).

Tsang, Y. W., The effect of tortuosity on fluid flow through a single fracture, *Water Resources Res.* **20**, 1209–1215 (1984).

Tsang, Y. W., and Tsang, C. F., Channel model of flow through fractured media, *Water Resources Res.* **23**, 467–479 (1987).

Tsang, Y. W., and Witherspoon, P. A., The dependence of fracture mechanical and fluid flow properties on surface roughness and sample size, *J. Geophys. Res.* **88**, 2359–2366 (1983).

Tsang, Y. W., and Tsang, C. F., Flow channeling in a single fracture as a two-dimensional strongly heterogeneous permeable medium, *Water Resources Res.* **25**, 2076–2080 (1989).

Voss, R. F., Fractals in nature: From characterization to simulation, in: *The Science of Fractal Images* (H. O. Peitgen, and D. Saupe, eds.), Springer-Verlag, New York, pp. 21–70 (1988).

Wang, J., and Narasimhan, T., Fractal and statistical characterization of rough fractures, in: *Proceedings, Second Berkeley Symposium on Topics in Petroleum Engineering*, Berkeley, Lawrence Berkeley Laboratory, University of California, March 9–10, 1988, LBL-24337, pp. 33–38 (1988).

Wang, J. S. Y., Narasimhan, T. N., and Scholz, C. H., Aperture correlation of a fractal fracture, *J. Geophys. Res.* **93**, 2216–2224 (1988).

Walsh, J. B., Seismic wave attenuation in rock due to friction, *J. Geophys. Res.* **71**, 2591–2599 (1966).

Walsh, J. B., Effect of pore pressure and confining pressure on fracture permeability, *Internat. J. Rock Mech. Mining Sci. Geomech. Abstr.* **18**, 429–435 (1981).

Walsh, J. B., and Grosenbaugh, M. A., A new model for analyzing the effect of fractures on compressibility, *J. Geophys. Res.* **84**, 3532 (1979).

White, J. E., *Underground Sound, Application of Seismic Waves*, Elsevier, New York (1983).

Witherspoon, P. A., Amick, C. H., Gale, J. E., and Iwai, K., Observations of a potential size effect in experimental determination of the hydraulic properties of fractures, *Water Resources Res.* **15**, 1142 (1979).

Witherspoon, P. A., Wang, J. S. Y., Iwai, K., and Gale, J. E., Validity of cubic law for fluid flow in a deformable rock fracture, *Water Resources Res.* **16**, 1016–1024 (1980).

Yang, G., Cook, N. G. W., and Myer, L. R., Network modeling of flow in natural fractures, in: *Proceedings, Rock Mechanics: Proceedings of the 30th U. S. Symposium*, Morganstown, West Virginia, June 19–22, 1989, University of West Virginia (1989).

Yoshioka, N., and Scholz, C. H., Elastic properties of contacting surfaces under normal and shear loads: Comparison of theory with experiment, *J. Geophys. Res.* **94**, 17691–1770 (1989).

Yu, T. R., and Telford, W. M., An ultrasonic system for fracture detection in rock faces, *Canad. Mining Metallurgy Bull.* **66**, 96–101 (1973).